Orbital and interlayer Skyrmions crystals in bilayer graphene

R. Côté,[1] Wenchen Luo,[1] Branko Petrov,[1] Yafis Barlas,[2] and A. H. MacDonald[3]

[1]*Département de physique, Université de Sherbrooke, Sherbrooke, Québec, J1K 2R1, Canada*
[2]*National High Magnetic Field Laboratory and Department of Physics,*
The Florida State University, Tallahassee, Florida 32306, USA
[3]*Department of Physics, The University of Texas at Austin, Austin, Texas 78712, USA*
(Dated: October 5, 2010)

A graphene bilayer in a transverse magnetic field has a set of Landau levels with energies $E = \pm\sqrt{N(N+1)}\hbar\omega_c^*$ where ω_c^* is the effective cyclotron frequency and $N = 0, 1, 2, ...$ All Landau levels but $N = 0$ are four times degenerate counting spin and valley degrees of freedom. The Landau level $N = 0$ has an extra degeneracy due to the fact that orbitals $n = 0$ and $n = 1$ both have zero kinetic energies. At integer filling factors, Coulomb interactions produce a set of broken-symmetry states with partial or full alignement in space of the valley and orbital pseudospins. These quantum Hall pseudo-ferromagnetic states support topological charged excitations in the form of orbital and valley Skyrmions. Away from integer fillings, these topological excitations can condense to form a rich variety of Skyrme crystals with interesting properties. We study in this paper different crystal phases that occur when an electric field is applied between the layers. We show that orbital Skyrmions, in analogy with spin Skyrmions, have a texture of electrical dipoles that can be controlled by an in-plane electric field. Moreover, the modulation of electronic density in the crystalline phases are experimentally accessible through a measurement of their local density of states

PACS numbers: 73.21.-b,73.22.Gk,78.70.Gq

I. INTRODUCTION

Bilayer graphene is a system consisting of two layers of graphene separated by a distance $d = 3.337$ Å. In the Bernal stacking structure, one of the two honeycomb sublattice sites in each layer has a near neighbor in the other layer and one does not. In a transverse magnetic field, the two-dimensional electron gas (2DEG) develops a set of Landau levels with energies $E^0 = \pm\sqrt{N(N+1)}\hbar\omega_c^*$ where $N = 0, 1, 2, ...$ and $\omega_c^* = eB/m^*c$ is the effective cyclotron frequency. The effective mass given by $m^* = 2\hbar^2\gamma_1/3\gamma_0^2 a_0^2$ where a_0 is the lattice constant of graphene and γ_0 and γ_1 are in-plane nearest-neighbor and inter-plane hopping parameters. By comparison, the effective mass is zero in graphene and the Landau levels energies are then given by $E^0 = \pm\sqrt{2}\hbar v_F\sqrt{N}/\ell$ where $\ell^2 = \hbar c/eB$ is the magnetic length and $v_F = \sqrt{3}a_0\gamma_0/2\hbar$ is the Fermi velocity.

In the absence of an electric field between the layers and Zeeman coupling, the Landau level $N = 0$ in a graphene bilayer contains 8 states for each guiding center orbital. The extra degeneracy is due to the fact that *orbitals* (we define this term in the next section) $n = 0$ and $n = 1$ both have the same kinetic energy $E = 0$. Consequently, an electron in $N = 0$ must be described by its spin, valley (or layer), and orbital quantum numbers in addition to its guiding center index X in the Landau gauge. When Coulomb interaction is considered, this extra degeneracy produces a rich phase diagram for the bilayer graphene's 2DEG. More so, in fact, than in a semiconductor 2DEG. In a series of related papers[1–3], we have shown that the octet degeneracy is lifted by the Coulomb interaction. The broken-symmetry ground states that emerge can be described as quantum Hall

pseudo-ferromagnets in the pseudospin language where fictitious spins are associated with the valley and orbital indices. These new states have interesting transport properties such as an intra-Landau-level cyclotron mode and a layer pseudospin with a quadratic ($\omega \sim q^2$) dispersion implying a vanishing superfluid density.

It is well known that a quantum Hall ferromagnet (QHF) in a usual semiconductor 2DEG has topological excitations named spin Skyrmions[4]. A single Skyrmion spin texture has its spins aligned with the Zeeman field at infinity, reversed at the center of the Skyrmion, and has non zero XY spin components at intermediate distance which have a vortex-like configuration. Skyrmions carry electric charge. Calculations have shown that Skyrmion-anti-Skyrmion pairs have lower energy than electron-hole quasiparticles near filling factor $\nu = 1$ and dominate the transport properties of the QHF[5]. A quantum Hall bilayer has, in addition to spin Skyrmions, topological excitations named pseudospin Skyrmions where the fictitious spin is associated with the layer index. We show in this paper that, in a graphene bilayer, there is a third possibility: that of an orbital-pseudospin Skyrmion. This quasiparticle has an associated electric dipole texture in the plane of the layers and can be seen as the analog of a spin Skyrmion who carries a magnetic texture.

We present several crystal states with pseudospin texture that occur near integer filling factors in Landau level $N = 0$. We assume full spin polarization of the 2DEG and concentrate on Skyrme crystals with valley and/or orbital pseudospin textures. We allow for the presence of an electric field between the layers that creates a charge imbalance and we study the evolution of the Skyrme crystals as a function of this electrical "bias" for different filling factors. Our goal is not to study the full phase diagram

of the bilayer but to focus on a small number of interesting crystal phases that are likely to occur near integer filling factors. Our calculation shows that Skyrmions tend to crystallize in pairs and that an orbital-pseudospin texture is favored over valley-pseudospin texture at filling factors $\nu = -3, -1, 1, 3$. Valley-pseudospin Skyrmion crystals occur at filling factor $\nu = -2, 2$ and involve a texture in both the $n = 0$ and $n = 1$ orbitals. This possibility was discussed before, for an isolated Skyrmion, in Ref. 6. We also show that Skyrmions with different electric charge q can be distinguished on the basis of their density of states. Moreover, the real-space density pattern of a Skyrmion crystal is accessible by a measurement of its local density of states.

This paper is organized as follows. In Sec. II, we present the effective two-band tight-binding model that we use to describe the graphene bilayer. In Sec. III, we derive the Hamiltonian of the bilayer graphene's 2DEG in the Hartree-Fock approximation. Sec. IV presents the pseudospin language used to describe the various crystal phases. In Sec. V, we introduce spin and orbital-pseudospin Skyrmions. We then present and discuss various Skyrmion crystal phases at filling factors $\nu = -3, -2, -1$ (or equivalently $\nu = 1, 2, 3$) in Sec. VI. The total and local densities of states are defined in Sec. VII and calculated for some of the crystal phases. The electric dipole texture associated with an orbital Skyrmion crystal is computed in Sec. VIII. We conclude in Sec. IX with a discussion of some of the terms neglected in our simple tight-binding model.

II. EFFECTIVE HAMILTONIAN

We consider the graphene bilayer in the Bernal stacking arrangement[7] represented in Fig. 1. We denote the two basis atoms of the top layer by A_1 and B_1 and those of the bottom layer by A_2 and B_2 with atoms A_1 situated directly above atoms B_2. The bilayer is placed in an external transverse electric field in order to control the electrical potential difference (i.e. the "bias") Δ_B between the layers that causes the charge imbalance. To simplify our analysis, we assume complete spin polarization of the electron gas and neglect trigonal warping (the γ_3 hopping in Fig. 1). We also use an effective two-band model[8] to describe the low-energy excitations of the bilayer in a quantizing magnetic field in the valleys $\mathbf{K} = (-4\pi/3a_0, 0)$ and $\mathbf{K}' = (4\pi/3a_0, 0)$. Although we will not consider these terms in the bulk of this paper, we could generalize this model by including the γ_4 hopping term as well as an additional term Δ representing the difference in the crystal field experienced by the inequivalent atoms A and B in the same plane. With these approximations, we get the Hamiltonian:

$$H_K^0 = \begin{pmatrix} -\frac{\Delta_B}{2} + (\beta_0 \Delta_B + \zeta_1) aa^\dagger & \zeta_2 a^2 \\ \zeta_2 (a^\dagger)^2 & \frac{\Delta_B}{2} + (-\beta_0 \Delta_B + \zeta_1) a^\dagger a \end{pmatrix},$$
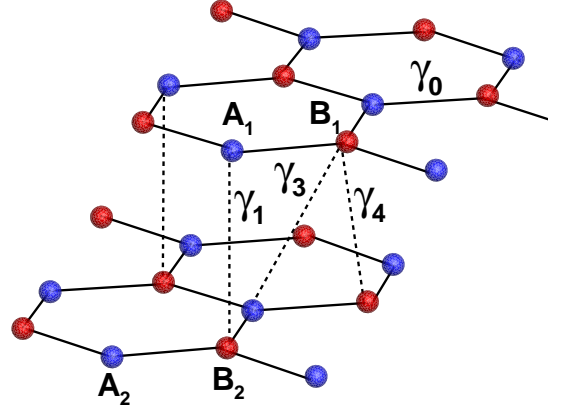
(1)

FIG. 1: (Color online) Crystal structure and definition of the hopping parameters for the graphene bilayer.

in the basis (A_2, B_1). In Eq. (1), $a, a^\dagger$ are the ladder operators for the Landau levels and we have defined the parameters

$$\zeta_1 = 2\mathrm{sgn}(\gamma_0 \gamma_4) \sqrt{\beta_0 \beta_4} \gamma_1 + (\beta_0 + \beta_4) \Delta, \quad (2)$$

$$\zeta_2 = 2\mathrm{sgn}(\gamma_0 \gamma_4) \sqrt{\beta_0 \beta_4} \Delta + (\beta_0 + \beta_4) \gamma_1, \quad (3)$$

where

$$\beta_0 = \frac{\hbar \omega_c^*}{\gamma_1}, \quad (4)$$

$$\beta_4 = \left(\frac{\gamma_4}{\gamma_0}\right)^2 \frac{\hbar \omega_c^*}{\gamma_1}, \quad (5)$$

are unitless constants and sgn denotes the signum function. The effective cyclotron frequency is defined by $\omega_c^* = eB/m^*c$ with the effective electronic mass given by $m^* = 2\hbar^2 \gamma_1/3\gamma_0^2 a_0^2 = 0.054 m_0$ where m_0 is the bare electronic mass and $a_0 = 2.46$ Å is the lattice parameter of graphene. Note that, in the basis (A_2, B_1), $H_{K'}^0 = (H_K^0)^\dagger$.

In the case where $\gamma_4 = \Delta = \Delta_B = 0$, the Landau level energies are given by

$$E^0 = \pm\sqrt{N(N+1)}\hbar\omega_c^*, \quad (6)$$

with $N = 0, 1, 2, 3, ...$ All Landau levels are four time degenerate (including spin and valley degrees of freedom) with the exception of $N = 0$ that is eight times degenerate. With finite $\gamma_4, \Delta, \Delta_B$, we find for the spin up states of $N = 0$ the following spinors and energies:

$$\begin{pmatrix} 0 \\ h_{0,X}(\mathbf{r}) \end{pmatrix}, \quad E_{K,0,X}^0 = \frac{1}{2}\Delta_B, \quad (7)$$

$$\begin{pmatrix} 0 \\ h_{1,X}(\mathbf{r}) \end{pmatrix}, \quad E_{K,1,X}^0 = \frac{1}{2}\Delta_B - \beta_0 \Delta_B + \zeta_1, \quad (8)$$

for the K valley and

$$\begin{pmatrix} h_{0,X}\left(\mathbf{r}\right) \\ 0 \end{pmatrix}, \; E^0_{K',0,X} \;=\; -\frac{1}{2}\Delta_B, \tag{9}$$

$$\begin{pmatrix} h_{1,X}\left(\mathbf{r}\right) \\ 0 \end{pmatrix}, \; E^0_{K',1,X} \;=\; -\frac{1}{2}\Delta_B + \beta_0\Delta_B + \zeta_1, \tag{10}$$

for the K' valley. Note that we have neglected the Zeeman coupling since we assume complete spin polarization and thus discard the spin degree of freedom in the rest of our analysis. The functions $h_{n,X}\left(\mathbf{r}\right) = e^{-iXy/\ell^2}\varphi_n\left(x-X\right)/\sqrt{L_y}$ are the eigenstates in the Landau gauge $\mathbf{A} = (0, Bx, 0)$ with guiding center X and $\varphi_n\left(x\right)$ is the wave function of the one-dimensional harmonic oscillator. The magnetic length is given by $\ell = \sqrt{\hbar c/eB} = 256/\sqrt{B}$ Å. We see from Eqs. (7-8) that, in addition to the spin and valley quantum numbers, there is in $N=0$ an extra degeneracy due to the fact that wave functions $h_{0,X}\left(\mathbf{r}\right)$ and $h_{1,X}\left(\mathbf{r}\right)$ both have zero kinetic energy if $\Delta_B = 0$. Throughout this paper, we will refer to these states as *orbitals* $n = 0, 1$ and use the symbol N for the Landau level index.

From Eqs. (7)-(10), we see that, in the Landau level $N=0$, the electrons are localized on the atoms A_2 (bottom layer) in the K' valley and on the atoms B_1 (top layer) in the K valley. In $N=0$, the layer index is equivalent to the valley index. An external electric field lifts both the valley and the orbital degeneracies. The orbital degeneracy is lifted by the small corrections $\beta_0\Delta_B$ and ζ_1 as shown in Fig. 2. The values of the intra and interlayer hoppings are given by $\gamma_0 = 3.12$ eV and $\gamma_1 = 0.39$ eV. The other hopping terms as well as Δ are not so well known. It is difficult to get the relative signs of these terms from the litterature. Recent measurements of these parameters for bilayer graphene give $\gamma_4 = 0.04 - 0.07$ and $\Delta = 0.005 - 0.008$ in units of the in-plane hopping γ_0. These values are discussed and referenced in Ref. 9. Taking the minimal values for γ_4 and Δ, we have $\beta_0 = 8.86 \times 10^{-3}B$, $\beta_4 = 1.31 \times 10^{-5}B$ (with the magnetic field in Tesla) and $\Delta = 0.0156$ eV so that $\zeta_1 = 4.042 \times 10^{-4}B$ eV.

We showed in Refs. 1–3 that when $\zeta_1 = 0$, the phase diagram of the 2DEG at integer filling factors $\nu \in [-3, 4]$ contains phases with interlayer and/or inter-orbital coherences. Because of the small interlayer spacing ($d = 3.337$ Å) in a graphene bilayer, interlayer coherence is rapidly lost when Δ_B increases i.e. for $\Delta_B/\left(e^2/\kappa\ell\right) \gtrsim 0.001$ according to our numerical calculations (κ is the effective dielectric constant at the position of the graphene layers). Above this value, inter-orbital coherence sets in when $E^0_{K,0,X} > E^0_{K,1,X}$. From Eqs. (9-10), this is only possible at $\nu = -1, 3$. Indeed, our calculations show that the phase diagram for $\nu = -3, 1$ has no orbital-coherent phase (when $\zeta_1 = 0$) if the band parameters we use are correct.

The precise values of the bias for the transitions between the different liquid phases at integer filling factors are very sensitive to the exact values of the hopping parameters. The same is true for the boundaries between various crystal phases at non-integer filling factors. Moreover, the number of possible crystal phases is much larger than the number of possible liquid phases when one considers the various crystal lattices and the possibility of having more than one electron per unit cell with interlayer and/or orbital pseudospin textures. For this reason, we focus, in this paper, on the analysis of a few crystal phases with orbital or interlayer texture which are likely to appear in the phase diagram of the 2DEG in some range of values of ζ_1. We assume $\zeta_1 = 0$ for all our calculations and discuss in the conclusion how the phase diagram is likely to be changed when $\zeta_1 \neq 0$. In our opinion reliable determination of the phase boundary characterizing the many possible crystalline phases will require experimental input.

Note that in the absence of Landau level mixing and when maximal spin polarization is assumed, the ground states at filling factors $\nu = -3, -2, -1$ are equivalent to those at filling factors $\nu = 1, 2, 3$. It is thus sufficient for us to study the first three states $\nu = -3, -2, -1$. If the approximation of maximal spin polarization is not made, phases with reduced polarization become possible as the bias is increased. (The energy of half the spin down (up) states decreases (increases) with bias and levels crossing do occur). The ground states at $\nu = -3, -2, -1$ are no longer equivalent to those at $\nu = 1, 2, 3$. The phase diagram is much more complex in this case but our calculations show that phases with orbital or interlayer coherences are still present.
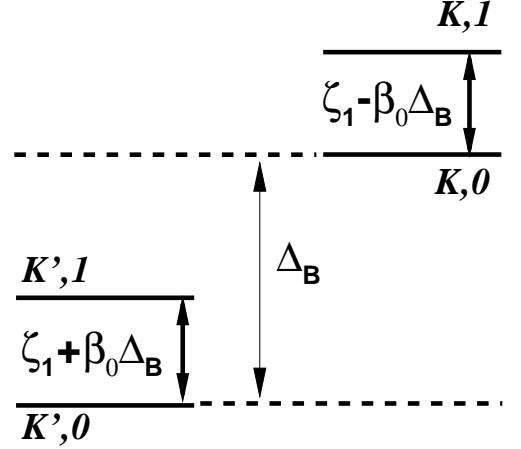

FIG. 2: Non-interacting energy levels with spin up in Landau level $N = 0$. Note that when $\zeta_1 = 0$, level $K, 1$ is below level $K, 0$ in energy.

III. HARTREE-FOCK DESCRIPTION OF THE CRYSTAL PHASES

We now add the Coulomb interaction to the non-interacting Hamiltonian. We assume that the magnetic field is strong enough so that we can neglect Landau level mixing. The Hartree-Fock Hamiltonian for the 2DEG in Landau level $N = 0$ is then given by

$$H_{HF} = N_\varphi \sum_n \sum_a E_{a,n} \rho^{a,a}_{n,n}(0) \tag{11}$$

$$+ N_\varphi \sum_{a,b} \sum_{n_1,\ldots,n_4} \overline{\sum_\mathbf{q}} H^{a,b}_{n_1,n_2,n_3,n_4}(\mathbf{q})$$

$$\times \left\langle \rho^{a,a}_{n_1,n_2}(-\mathbf{q}) \right\rangle \rho^{b,b}_{n_3,n_4}(\mathbf{q})$$

$$- N_\varphi \sum_{a,b} \sum_{n_1,\ldots,n_4} \sum_\mathbf{q} X^{a,b}_{n_1,n_4,n_3,n_2}(\mathbf{q})$$

$$\times \left\langle \rho^{a,b}_{n_1,n_2}(-\mathbf{q}) \right\rangle \rho^{b,a}_{n_3,n_4}(\mathbf{q}),$$

where $N_\varphi = S/2\pi\ell^2$ is the Landau level degeneracy (S is the 2DEG area) and all energies are now measured in units of $e^2/\kappa\ell$. The single-particle energies $E_{a,n}$ include capacitive contributions and are defined by

$$E_{a,n} = \frac{1}{2} a \Delta_B - a \beta_0 \Delta_B n + \left[\frac{\widetilde{\nu}}{2} \frac{d}{\ell} - \widetilde{\nu}_a \frac{d}{\ell} \right] + \zeta_1, \tag{12}$$

with $a, b = \pm 1$ the valley (or equivalently layer) index and $n = 0, 1$ the orbital index. (Our convention is that $a = 1(-1)$ for the $K(K')$ valley). Because we work in Landau level $N = 0$ only, we define $\widetilde{\nu} = \nu + 4 \in [0, 8]$ as the number of filled levels in $N = 0$. In deriving Eq. (11), we have taken into account a neutralizing positive background and put the capacitive energy in the third term on the right-hand side of Eq. (12). It follows that the $\mathbf{q} = 0$ contribution is absent in the Hartree term of Eq. (11). This convention is indicated by the bar over the summation.

In Eq. (11), the density operator is defined by

$$\rho^{a,b}_{n_1,n_2}(\mathbf{q}) = \frac{1}{N_\varphi} \sum_{X_1,X_2} e^{-\frac{i}{2} q_x(X_1+X_2)} \tag{13}$$

$$\times c^\dagger_{a,X_1,n_1} c_{b,X_2,n_2} \delta_{X_1,X_2+q_y\ell^2},$$

where $c^\dagger_{a,X,n}$ creates an electron in the state (a, X, n) in the Landau gauge. The intralayer $(H, X = H^{a,a}, X^{a,a})$ and interlayer $\left(\widetilde{H}, \widetilde{X} = H^{a\neq b}, X^{a\neq b} \right)$ Hartree and Fock interactions are defined by

$$H_{n_1,n_2,n_3,n_4}(\mathbf{q}) = \frac{1}{q\ell} K_{n_1,n_2}(\mathbf{q}) K_{n_3,n_4}(-\mathbf{q}), \tag{14}$$

$$X_{n_1,n_2,n_3,n_4}(\mathbf{q}) = \int \frac{d\mathbf{p}\ell^2}{2\pi} H_{n_1,n_2,n_3,n_4}(\mathbf{p}) e^{i\mathbf{q}\times\mathbf{p}\ell^2}, \tag{15}$$

and

$$\widetilde{H}_{n_1,n_2,n_3,n_4}(\mathbf{q}) = H_{n_1,n_2,n_3,n_4}(\mathbf{q}) e^{-qd}, \tag{16}$$

$$\widetilde{X}_{n_1,n_2,n_3,n_4}(\mathbf{q}) = \int \frac{d\mathbf{p}\ell^2}{2\pi} \widetilde{H}_{n_1,n_2,n_3,n_4}(\mathbf{p}) e^{i\mathbf{q}\times\mathbf{p}\ell^2} \tag{17}$$

where $d = 3.337$ Å is the separation between the two graphene layers of the bilayer. The form factors which appear here,

$$K_{0,0}(\mathbf{q}) = \exp\left(\frac{-q^2\ell^2}{4} \right), \tag{18}$$

$$K_{1,1}(\mathbf{q}) = \exp\left(\frac{-q^2\ell^2}{4} \right) \left(1 - \frac{q^2\ell^2}{2} \right), \tag{19}$$

$$K_{1,0}(\mathbf{q}) = \left(\frac{(q_y + iq_x)\ell}{\sqrt{2}} \right) \exp\left(\frac{-q^2\ell^2}{4} \right), \tag{20}$$

$$K_{0,1}(\mathbf{q}) = \left(\frac{(-q_y + iq_x)\ell}{\sqrt{2}} \right) \exp\left(\frac{-q^2\ell^2}{4} \right), \tag{21}$$

capture the character of the two different orbital states. Detailed expressions for the Hartree and Fock interactions can be found in Appendix A of Ref. 3.

The average values of the density operators $\left\langle \rho^{a,b}_{n_1,n_2}(\mathbf{q}) \right\rangle$ are found by solving the Hartree-Fock equation of motion for the matrix Green's function

$$G^{a,b}_{n_1,n_2}(\mathbf{q},\tau) = \frac{1}{N_\varphi} \sum_{X,X'} e^{-\frac{i}{2} q_x(X+X')} \tag{22}$$

$$\times \delta_{X,X'-q_y\ell^2} G^{a,b}_{n_1,n_2}(X, X', \tau),$$

with

$$G^{a,b}_{n_1,n_2}(X, X', \tau) = -\left\langle T c_{a,X,n_1}(\tau) c^\dagger_{b,X',n_2}(0) \right\rangle. \tag{23}$$

When $\tau = 0^-$,

$$G^{a,b}_{n_1,n_2}(\mathbf{q}, \tau = 0^-) = \left\langle \rho^{b,a}_{n_2,n_1}(\mathbf{q}) \right\rangle. \tag{24}$$

The Hartre-Fock equation of motion for this single particle Green's function is given by

$$[\hbar i \omega_n - (E_{a,n} - \mu)] G^{a,b}_{n,n'}(\mathbf{q}, \omega_n) = \hbar \delta_{\mathbf{q},0} \delta_{n,n'} \delta_{a,b} \tag{25}$$

$$+ \sum_{c,n_4} \overline{\sum_{\mathbf{q}'}} U^H_{c,a}(n, n_4, \mathbf{q} - \mathbf{q}') e^{-i\mathbf{q}\times\mathbf{q}'\ell^2/2} G^{a,b}_{n_4,n'}(\mathbf{q}', \omega_n)$$

$$- \sum_{c,n_4} \sum_{\mathbf{q}'} U^F_{c,a}(n, n_4, \mathbf{q} - \mathbf{q}') e^{-i\mathbf{q}\times\mathbf{q}'\ell^2/2} G^{c,b}_{n_4,n'}(\mathbf{q}', \omega_n),$$

with the Hartree and Fock potentials

$$U^H_{c,a}(n, n_4, \mathbf{q}) = \sum_{n_1,n_2} H_{c,a}(n_1, n_2, n, n_4; -\mathbf{q}) \left\langle \rho^{c,c}_{n_1,n_2}(\mathbf{q}) \right\rangle, \tag{26}$$

$$U^F_{c,a}(n, n_4, \mathbf{q}) = \sum_{n_1,n_2} X_{c,a}(n_1, n_4, n, n_2; -\mathbf{q}) \left\langle \rho^{c,a}_{n_1,n_2}(\mathbf{q}) \right\rangle. \tag{27}$$

In these equations, $H_{c=a} = H$, $H_{c \neq a} = \widetilde{H}$ and similarly for $X_{c,a}$.

Equation (25) constitutes a set of self-consistent equations that can be solved numerically using the procedure described in Ref. 10. We search amongst the many solutions of this equation for the one that minimizes the Hartree-Fock energy per electron

$$
\begin{aligned}
\frac{E_{HF}}{N_0} = {} & \frac{1}{\widetilde{\nu}} \sum_{a,n} E_{a,n} \left\langle \rho_{n,n}^{a,a}(0) \right\rangle \qquad (28) \\
& + \frac{1}{2\widetilde{\nu}} \sum_{a,b} \sum_{n_1,...,n_4} \overline{\sum_{\mathbf{q}}} H_{a,b}(n_1, n_2, n_3, n_4; \mathbf{q}) \\
& \times \left\langle \rho_{n_1,n_2}^{a,a}(-\mathbf{q}) \right\rangle \left\langle \rho_{n_3,n_4}^{b,b}(\mathbf{q}) \right\rangle \\
& - \frac{1}{2\widetilde{\nu}} \sum_{a,b} \sum_{n_1,...,n_4} \sum_{\mathbf{q}} X_{a,b}(n_1, n_4, n_3, n_2; \mathbf{q}) \\
& \times \left\langle \rho_{n_1,n_2}^{a,b}(-\mathbf{q}) \right\rangle \left\langle \rho_{n_3,n_4}^{b,a}(\mathbf{q}) \right\rangle,
\end{aligned}
$$

where N_0 is the number of electrons in $N = 0$.

IV. ORDER PARAMETERS AND PSEUDOSPIN DESCRIPTION

The set of parameters $\left\{ \left\langle \rho_{n_1,n_2}^{a,b}(\mathbf{q}) \right\rangle \right\}$ fully characterizes a particular ground state. In the uniform states studied in Refs. 1–3, these parameters were nonzero for $\mathbf{q} = 0$ only. In this paper, however, we study crystal states occurring at non-integer filling factor $\widetilde{\nu}$ where we expect a finite fraction of the electrons, usually $\widetilde{\nu} - \lfloor \widetilde{\nu} \rfloor$, to crystallize. The set of parameters $\left\{ \left\langle \rho_{n_1,n_2}^{a,b}(\mathbf{q}) \right\rangle \right\}$ are then nonzero for $\mathbf{q} = \mathbf{G}$ where $\mathbf{G}$ is a reciprocal lattice vector of the crystal lattice considered.

Generally speaking, crystalline states should occur universally near integer filling factors in order to maximize the correlations among the lowest-energy elementary charged excitations. When the charged objects become more dense at larger departures from integer filling factor they will begin to overlap. Eventually the various exotic crystalline states will quantum melt and the electrons will form a fluid state. The methods employed in this paper are not able to predict the stability range of the crystalline states.

In Fourier space, the real electronic density in valley (or layer) a is given by

$$
\left\langle n_a(\mathbf{G}) \right\rangle = \sum_{n,m=0}^{1} N_\varphi K_{n,m}(-\mathbf{G}) \left\langle \rho_{n,m}^{a,a}(\mathbf{G}) \right\rangle. \qquad (29)
$$

We will refer to the inverse Fourier transform $n_a(\mathbf{r})$ of $\left\langle n_a(\mathbf{G}) \right\rangle$ as the density in the *real space representation* (RSR). We also make use of another expression for the density:

$$
\left\langle \widetilde{n}_a(\mathbf{G}) \right\rangle = \sum_{n=0}^{1} \left\langle \rho_{n,n}^{a,a}(\mathbf{G}) \right\rangle. \qquad (30)
$$

We refer to the inverse Fourier transform $\widetilde{n}_a(\mathbf{r})$ of $\left\langle \widetilde{n}_a(\mathbf{G}) \right\rangle$ as the density in the *guiding-center representation* (GCR). By definition, $\left\langle \widetilde{n}_a(\mathbf{G} = 0) \right\rangle = \widetilde{\nu}_a$ is just the filling factor in valley a. The form factors $K_{n,m}(\mathbf{G})$ are not taken into account in the GCR so that the character of the different orbitals $n = 0, 1$ is lost in the corresponding density.

Interlayer coherence implies that $\left\langle \rho_{n,n}^{a,b \neq a}(\mathbf{G}) \right\rangle \neq 0$ while inter-orbital coherence implies that $\left\langle \rho_{n,m \neq n}^{a,a}(\mathbf{G}) \right\rangle \neq 0$. In the most general case, both interlayer and inter-orbital coherences are present and $\left\langle \rho_{n,m \neq n}^{a,b \neq a}(\mathbf{G}) \right\rangle \neq 0$. The different phases are best described by using a pseudospin language. For the orbital pseudospin, $\mathbf{S}$, we associate the up state with the $n = 0$ orbital and the down state with the $n = 1$ orbital so that in valley a :

$$
\widetilde{S}_{a,z}(\mathbf{G}) = \frac{1}{2} \left[\left\langle \rho_{0,0}^{a,a}(\mathbf{G}) \right\rangle - \left\langle \rho_{1,1}^{a,a}(\mathbf{G}) \right\rangle \right], \qquad (31)
$$

$$
\widetilde{\mathbf{S}}_{a,\perp}(\mathbf{G}) = \widetilde{S}_{a,x}\widehat{\mathbf{x}} + \widetilde{S}_{a,y}\widehat{\mathbf{y}}, \qquad (32)
$$

$$
\widetilde{S}_{a,+}(\mathbf{G}) = \widetilde{S}_{a,x} + i\widetilde{S}_{a,y} = \left\langle \rho_{0,1}^{a,a}(\mathbf{G}) \right\rangle. \qquad (33)
$$

For the interlayer pseudospin, $\mathbf{P}$, we associate the up state with the K layer and the down state with the K' layer so that for orbital n, we have

$$
\widetilde{P}_{n,z}(\mathbf{G}) = \frac{1}{2} \left[\left\langle \rho_{n,n}^{K,K}(\mathbf{G}) \right\rangle - \left\langle \rho_{n,n}^{K',K'}(\mathbf{G}) \right\rangle \right], \quad (34)
$$

$$
\widetilde{\mathbf{P}}_{\perp,n}(\mathbf{G}) = \widetilde{P}_{n,x}\widehat{\mathbf{x}} + \widetilde{P}_{n,y}\widehat{\mathbf{y}}, \qquad (35)
$$

$$
\widetilde{P}_{n,+}(\mathbf{G}) = \widetilde{P}_{n,x} + i\widetilde{P}_{n,y} = \left\langle \rho_{n,n}^{K,K'}(\mathbf{G}) \right\rangle. \qquad (36)
$$

Note that these fields are defined in the GCR. To get them in the RSR, we multiply each $\left\langle \rho_{n,m}^{a,a}(\mathbf{G}) \right\rangle$ in these definitions with $N_\varphi K_{n,m}(-\mathbf{G})$. From now on, we use the notation $\widetilde{\mathbf{S}}, \widetilde{\mathbf{P}}, \widetilde{n}$ to refer to the fields in the GCR and the notation $\mathbf{S}, \mathbf{P}, n$ for the fields in the RSR. The two views give separate interesting insights into the nature of the crystal states, but the RSR is more closely related to experimental probes like a scanning tunneling microscope (STM).

An exact description of the state of one electron in $N = 0$ is given by the four complex components of the spinor $\left(c_{K,X,0}^\dagger, c_{K,X,1}^\dagger, c_{K',X,0}^\dagger, c_{K',X,1}^\dagger \right)$. Note that, in order to limit the range of possible states, we will restrict our attention to circumstances in which the $N = 0$ states are maximally polarized. As we mentioned in Sec. II, we expect that partially polarized states will be common at large interlayer potentials. The ideas explained here are readily generalized to include this possibility. For a CP^3 spinor, the norm and the absolute phase are fixed so that a given electronic state is defined by 6 independent components or angles[11]. The 12 classical fields $\widetilde{\mathbf{P}}_{n=0,1}(\mathbf{G})$, $\widetilde{\mathbf{S}}_{\pm K}(\mathbf{G})$ that we defined in Eqs. (31-36) have a simple physical interpretation but they do not provide a full description of a given phase. Moreover,

these fields are not independent variables and their norm is not fixed. Both the modulus and the orientation of these pseudospins may vary in space. In fact, the sum rule

$$\sum_{a,b}\sum_{n,m}\sum_{\mathbf{G}} \left| \left\langle \rho_{n,m}^{a,b}\left(\mathbf{G}\right)\right\rangle \right|^{2} = \widetilde{\nu}, \tag{37}$$

that applies when the many-electron state is approximated by a single Slater determinant becomes, in pseudospin language,

$$\sum_{\mathbf{G}} \left[\frac{1}{4} \left| \rho_{K}\left(\mathbf{G}\right) + \rho_{K'}\left(\mathbf{G}\right) \right|^{2} \right. \tag{38}$$
$$- \left| \widetilde{P}_{z,0}\left(\mathbf{G}\right) - \widetilde{P}_{z,1}\left(-\mathbf{G}\right) \right|^{2}$$
$$+ 2\left| \widetilde{S}_{K}\left(\mathbf{G}\right) \right|^{2} + 2\left| \widetilde{S}_{K'}\left(\mathbf{G}\right) \right|^{2}$$
$$+ 2\left| \widetilde{\mathbf{P}}_{0}\left(\mathbf{G}\right) \right|^{2} + 2\left| \widetilde{\mathbf{P}}_{1}\left(\mathbf{G}\right) \right|^{2}$$
$$\left. + 2\left| \left\langle \rho_{0,1}^{K,K'}\left(\mathbf{G}\right)\right\rangle \right|^{2} + 2\left| \left\langle \rho_{1,0}^{K,K'}\left(\mathbf{G}\right)\right\rangle \right|^{2} \right]$$
$$= \widetilde{\nu}.$$

, where we have defined $\rho_{a} = \rho_{0,0}^{a,a}$.

Skyrmion crystals with intervalley pseudospin textures have been studied extensively in semiconductor 2DEG as well as in graphene monolayers[12–14]. In bilayer graphene, we have the additional possibility of orbital pseudospin texture. This type of texture is particularly interesting because it gives rise to textures of electric dipoles in the plane of the layer. As shown in Refs. 3,15, the coupling of the 2DEG with an electric field $\mathbf{E}\left(\mathbf{r}\right) = -\nabla\phi\left(\mathbf{r}\right)$ in the plane of the layers can be written as $H_{ext} = -e\int d\mathbf{r}\, n\left(\mathbf{r}\right)\phi\left(\mathbf{r}\right)$ where $n\left(\mathbf{r}\right)$ is the Fourier transform of the total density $n_{K}\left(\mathbf{G}\right) + n_{K'}\left(\mathbf{G}\right)$ (see Eq. (29). With the form factor defined in Eqs. (18-21) and $j = K, K'$,

$$H_{ext} = -\frac{eN_{\varphi}}{S}\sum_{j}\sum_{\mathbf{G}} \left[\left(1 - \frac{G^{2}\ell^{2}}{4}\right) \overline{\rho}_{j}\left(-\mathbf{G}\right) \right. \tag{39}$$
$$+ \left(\frac{G^{2}\ell^{2}}{2}\right) \overline{\rho}_{j,z}\left(-\mathbf{G}\right)$$
$$\left. - \sqrt{2}i \left(G_{x}\ell\,\overline{\rho}_{j,x}\left(-\mathbf{G}\right) - G_{y}\ell\,\overline{\rho}_{j,y}\left(-\mathbf{G}\right)\right) \right] \phi\left(\mathbf{G}\right),$$

where we have defined $\overline{\rho}_{j}\left(\mathbf{G}\right) = \exp\left(-G^{2}\ell^{2}/4\right)\rho_{j}\left(\mathbf{G}\right)$. In real space,

$$H_{ext} = -eN_{\varphi}\sum_{j} \int d\mathbf{r} \left[\overline{\rho}_{j}\left(\mathbf{r}\right)\phi\left(\mathbf{r}\right) \right.$$
$$- \frac{1}{4} \left(\overline{\rho}_{j}\left(\mathbf{r}\right)\ell^{2} - 2\overline{\rho}_{j,z}\left(\mathbf{r}\right)\ell^{2} \right) \left(\nabla\cdot\mathbf{E}\left(\mathbf{r}\right)\right) \right] \tag{40}$$
$$+ \sqrt{2}\ell eN_{\varphi} \int d\mathbf{r} \left[\overline{\rho}_{j,x}\left(\mathbf{r}\right)E_{x}\left(\mathbf{r}\right) - \overline{\rho}_{j,y}\left(\mathbf{r}\right)E_{y}\left(\mathbf{r}\right) \right],$$

so that we can identify

$$\mathbf{d}_{a}\left(\mathbf{G}\right) = -e\sqrt{2}\ell N_{\varphi}e^{-G^{2}\ell^{2}/4} \tag{41}$$
$$\times \left(\left\langle \rho_{a,x}\left(\mathbf{G}\right)\right\rangle \widehat{\mathbf{x}} - \left\langle \rho_{a,y}\left(\mathbf{G}\right)\right\rangle \widehat{\mathbf{y}} \right)$$

with the Fourier transform of an electric dipole field in layer a. The orientation of the dipole vector at each point in space is simply related to the orientation of the orbital pseudospin vector. It follows that crystals with orbital pseudospin textures then have electric-dipole textures. Orbital Skyrmion crystals are the electric analog of spin Skyrmions crystals in which it is the magnetization that varies in space. Note that in a uniform electric field, the second term in Eq. (40) is zero and H_{ext} gives the monopole and dipole terms of the interaction energy of the electrons with the external electric field.

V. ISOLATED SKYRMIONS

Before we can analyze the results of the numerical calculations for the Skyrmion crystal states, we need to know the density and pseudospin patterns associated with a single orbital Skyrmion located at $\mathbf{r} = 0$. We use, in this section, the symmetric gauge which is more convenient for this problem. We take $\mathbf{A} = \left(-By/2, Bx/2, 0\right)$ for the vector potential. The eigenfunctions of the kinetic Hamiltonian $H = \left(\mathbf{p} + e\mathbf{A}/c\right)^{2}/2m_{0}$ (where $-e$ is the charge of an electron and m_{0} the electronic mass) are given by

$$h_{n=0,m}\left(\mathbf{r}\right) = \frac{1}{\sqrt{2\pi 2^{m}m!}\ell} \left(\frac{r}{\ell}\right)^{m} e^{-im\varphi}e^{-r^{2}/4\ell^{2}}, \tag{42}$$

with $m = 0, 1, 2, ...$ for Landau level $n = 0$ and by

$$h_{n=1,m}\left(\mathbf{r}\right) = \frac{1}{\sqrt{\pi 2^{|m|+1}(m+1)!}}\frac{1}{\ell}\left(\frac{r}{\ell}\right)^{|m|} \tag{43}$$
$$\times e^{-im\varphi}e^{-r^{2}/4\ell^{2}}L_{1+\left(\frac{m-|m|}{2}\right)}^{|m|}\left(\frac{r^{2}}{2\ell^{2}}\right),$$

with $m = -1, 0, 1, 2, ...$for Landau level $n = 1$ and $L_{n}^{m}\left(x\right)$ is a generalized Laguerre polynomial. (Note that $h_{n,m}$ is a different function than $h_{n,X}$ introduced previously). Figure 3 shows the density profile $n_{1}\left(\mathbf{r}\right) = \left|h_{1,m}\left(\mathbf{r}\right)\right|^{2}$ for the eigenstates with $m = -1, 0, 1$.

The index $m \geq -n$ gives the angular momentum i.e.

$$L_{z}h_{n,m}\left(\mathbf{r}\right) = -\hbar m h_{n,m}\left(\mathbf{r}\right), \tag{44}$$

while the energy of each state (n, m) is given by

$$E_{n}^{0} = \left(n + 1/2\right)\hbar\omega_{c}, \tag{45}$$

where ω_{c} is the cyclotron frequency. Note that for a filled level, we have

$$n_{0}\left(\mathbf{r}\right) = \sum_{m=0}^{\infty} \left|h_{0,m}\left(\mathbf{r}\right)\right|^{2} = \frac{1}{2\pi\ell^{2}}, \tag{46}$$

$$n_{1}\left(\mathbf{r}\right) = \sum_{m=-1}^{\infty} \left|h_{1,m}\left(\mathbf{r}\right)\right|^{2} = \frac{1}{2\pi\ell^{2}}. \tag{47}$$
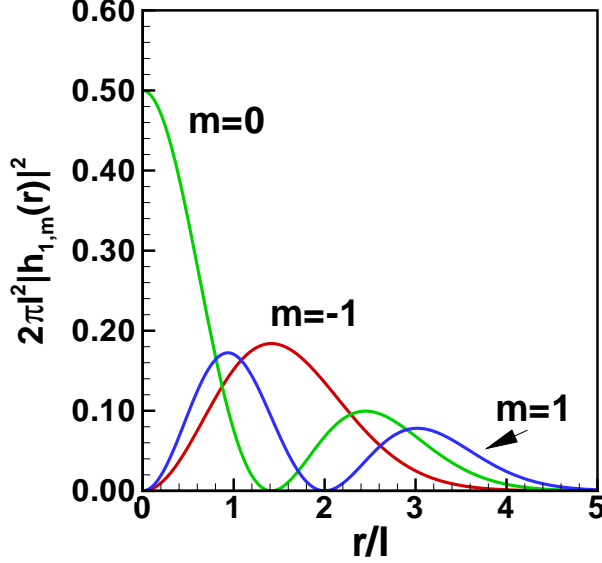
FIG. 3: (Color online) Density profile for the wave functions in $n = 1$ with $m = -1, 0, 1$.

A. Spin Skyrmion

In a semiconductor 2DEG, the state $|\mathcal{S}\rangle$ corresponding to the addition of one spin Skyrmion with topological charge $Q = 1$ at $\mathbf{r} = 0$ to the spin-polarized ground state $|GS\rangle = \prod_{m=0}^{\infty} c_{m,\uparrow}^{\dagger} |0\rangle$ at $\nu = 1$ (Landau level $N = 0$ is implicitly assumed) is given by

$$|\mathcal{S}\rangle = \prod_{m=0}^{\infty} \left[-u_m c_{\downarrow,m+1}^{\dagger} + v_m c_{\uparrow,m}^{\dagger} \right] c_{\downarrow,0}^{\dagger} |0\rangle, \qquad (48)$$

with the constraint that

$$|u_m|^2 + |v_m|^2 = 1. \qquad (49)$$

The anti-Skyrmion state is given by

$$|\mathcal{AS}\rangle = \prod_{m=0}^{\infty} \left[u_m c_{\downarrow,m}^{\dagger} + v_m c_{\uparrow,m+1}^{\dagger} \right] |0\rangle. \qquad (50)$$

The values of u_m and v_m depend on details on the Zeeman coupling and the electron-electron interaction and can be fixed by energy minimization.

The excitations $|\mathcal{S}\rangle, |\mathcal{AS}\rangle$ have collective coherence between single-particle states with different spins and angular momenta values that differ by one. The RSR of the field $\mathbf{S}_-(\mathbf{r}) = S_x(\mathbf{r}) - iS_y(\mathbf{r})$ for the Skyrmion state is given by

$$S_-(\mathbf{r}) = \langle \mathcal{S} | \Psi_{\downarrow}^{\dagger}(\mathbf{r}) \Psi_{\uparrow}(\mathbf{r}) | \mathcal{S} \rangle \qquad (51)$$

$$= -\sum_{m=0}^{\infty} h_{0,m+1}^*(\mathbf{r}) h_{0,m}(\mathbf{r}) u_m^* v_m,$$

where $\Psi_{\sigma}^{\dagger}(\mathbf{r})$ is the field operator that creates an electron at $\mathbf{r}$ with spin σ. The corresponding density of the two spin components in the RSR are then

$$n_{\uparrow}(\mathbf{r}) = \langle \mathcal{S} | \Psi_{\uparrow}^{\dagger}(\mathbf{r}) \Psi_{\uparrow}(\mathbf{r}) | \mathcal{S} \rangle \qquad (52)$$

$$= \sum_{m=0}^{\infty} |h_{0,m}(\mathbf{r})|^2 |v_m|^2,$$

and

$$n_{\downarrow}(\mathbf{r}) = \langle \mathcal{S} | \Psi_{\downarrow}^{\dagger}(\mathbf{r}) \Psi_{\downarrow}(\mathbf{r}) | \mathcal{S} \rangle \qquad (53)$$

$$= |h_{0,0}(\mathbf{r})|^2 + \sum_{m=0}^{\infty} |h_{0,m+1}(\mathbf{r})|^2 |u_m|^2.$$

The total density is of course

$$n(\mathbf{r}) = n_{\uparrow}(\mathbf{r}) + n_{\downarrow}(\mathbf{r}), \qquad (54)$$

while the $z-$component of the spin field is given by

$$S_z(\mathbf{r}) = \frac{1}{2} [n_{\uparrow}(\mathbf{r}) - n_{\downarrow}(\mathbf{r})]. \qquad (55)$$

(Note that for a filled level, $|S_z(\mathbf{r})| = 1/4\pi\ell^2$.)

Figure 4 shows the density and spin patterns for a spin Skyrmion with $Q = 1$ added to a filled Landau level. We have chosen for this figure the simple expression

$$u_m = \sqrt{\frac{\Delta}{m + 10 + \Delta}}, v_m = \sqrt{\frac{m + 10}{m + 10 + \Delta}}, \qquad (56)$$

where Δ is the Skyrmion size. This expression gives a density and pseudospin pattern for the Skyrmion which is qualitatively close to that given by the energy minimization[5]. Note that all spin and pseudospin densities in this figure and the subsequent ones in this paper are in units of $1/2\pi\ell^2$. This corresponds to the density of a filled Landau level (see Eqs. (46,47)).

B. Orbital Skyrmion

We now consider the case where all electrons have spin up and we try to make an orbital Skyrmion by flipping some orbital pseudospins from $n = 0$ to $n = 1$. For simplicity, we assume full valley and spin polarization so that we can drop the layer and spin indices. Full valley polarization is expected at all odd integer filling factors when the interlayer potential is strong. The ground state at $\widetilde{\nu} = 1$ is given by

$$|GS\rangle = \prod_{m=0}^{\infty} c_{0,m}^{\dagger} |0\rangle. \qquad (57)$$

An orbital anti-Skyrmion state can be written as

$$|\mathcal{AS}\rangle = \prod_{m=-1}^{\infty} \left[u_m c_{1,m}^{\dagger} + v_m c_{0,m+2}^{\dagger} \right] |0\rangle. \qquad (58)$$
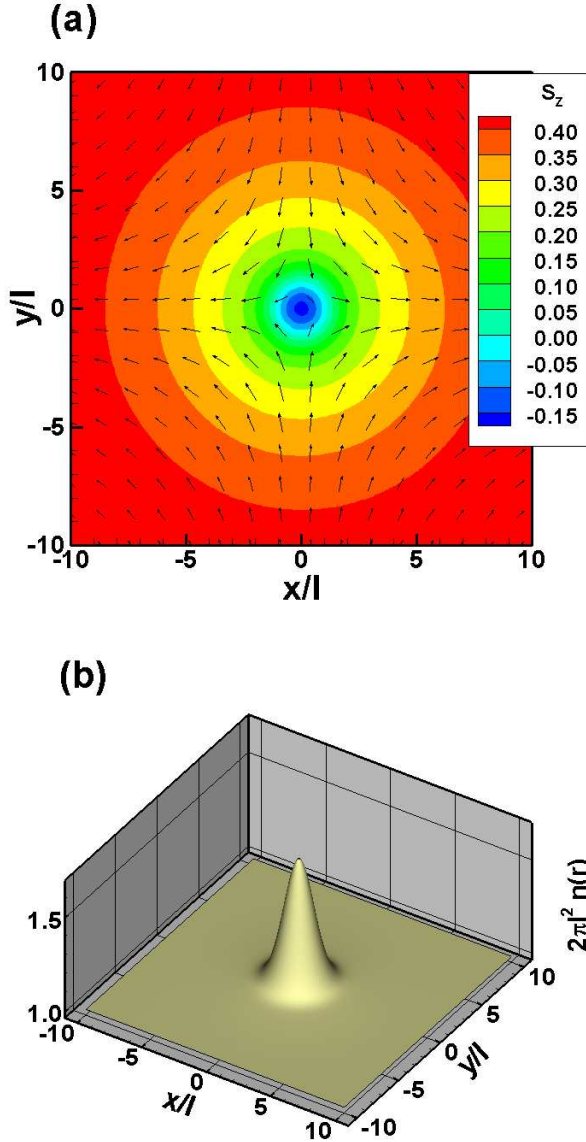
(a)

(b)

FIG. 4: (Color online) A charge $Q = 1$ Skyrmion for the parameters of Eq. (56) with $\Delta = 4$. (a) Spin profile in $x - y$ plane. (b) Total density $n(\mathbf{r})$.

We see that the angular momentum difference $\Delta m = m_1 - m_0 = -2$ because the lowest value of m in $n = 1$ is $m = -1$.

For the Skyrmion excitation with the same vorticity, we have three choices corresponding to $p = -1, 0, 1$ in the expression

$$|\mathcal{S}_p\rangle = \prod_{m=0}^{\infty} \left[-u_m c_{1,m+2}^{\dagger} + v_m c_{0,m}^{\dagger} \right] c_{1,p}^{\dagger} |0\rangle . \qquad (59)$$

The RSR of the pseudospin field $\mathbf{S}_-(\mathbf{r})$ is given by

$$S_-(\mathbf{r}) = -\sum_{m=0}^{\infty} h_{1,m+2}^*(\mathbf{r}) h_{0,m}(\mathbf{r}) u_m^* v_m, \qquad (60)$$

while the densities in $n = 0$ and $n = 1$ are given by

$$
\begin{aligned}
n_0(\mathbf{r}) &= \langle \mathcal{S}_p | \Psi_0^{\dagger}(\mathbf{r}) \Psi_0(\mathbf{r}) | \mathcal{S}_p \rangle \qquad (61) \\
&= \sum_{m=0}^{\infty} |h_{0,m}(\mathbf{r})|^2 |v_m|^2 ,
\end{aligned}
$$

and

$$
\begin{aligned}
n_{1,p}(\mathbf{r}) &= \langle \mathcal{S}_p | \Psi_1^{\dagger}(\mathbf{r}) \Psi_1(\mathbf{r}) | \mathcal{S}_p \rangle \qquad (62) \\
&= |\phi_{1,p}(\mathbf{r})|^2 + \sum_{m=0}^{\infty} |h_{1,m+2}(\mathbf{r})|^2 |v_m|^2 .
\end{aligned}
$$

For the orbital Skyrmion, the *total* density is given by

$$
\begin{aligned}
n(\mathbf{r}) &= \sum_{i,j=0}^{1} \langle \mathcal{S}_p | \Psi_i^{\dagger}(\mathbf{r}) \Psi_j(\mathbf{r}) | \mathcal{S}_p \rangle \qquad (63) \\
&= n_0(\mathbf{r}) + n_{1,p}(\mathbf{r}) + 2\mathrm{Re}\left[S_-(\mathbf{r}) \right]
\end{aligned}
$$

and includes the extra contribution $2\mathrm{Re}\left[S_-(\mathbf{r}) \right]$.

For the $z-$component

$$S_z(\mathbf{r}) = \frac{1}{2}\left[n_0(\mathbf{r}) - n_{1,p}(\mathbf{r}) \right]. \qquad (64)$$

To give an example, we take $p = -1$ and choose again Eq. (56) with $\Delta = 0.05$. The total density and pseudospin patterns are represented in Fig. 5. These patterns differ markedly from those of a spin Skyrmion. The coupling $m_1 - m_0 = -2$ between the angular momenta in $n = 0$ and $n = 1$ makes the orbital-pseudospin vector to rotate by 4π instead of 2π around the Skyrmion center. Because the value of u_m is small, the profile of the z-component of $S_z(\mathbf{r})$ is basically the (inverted) density profile $n_1(\mathbf{r})$ (see Fig. 3). Also, the total density $n(\mathbf{r})$ is anisotropic. Comparing this profile with that of $N_p(\mathbf{r}) \equiv n_0(\mathbf{r}) + n_{1,p}(\mathbf{r})$ (not shown in the figure) which is isotropic, we understand that the anisotropy comes from the term $2\mathrm{Re}\left[S_-(\mathbf{r}) \right]$ in Eq. (63). The density profile is typical of the density pattern of an electron in state $n = 0, p = -1$ (see Fig. 3).

Our choice for the u_m, v_m in this example is motivated by the fact that it reproduces qualitatively the density we observed in the crystal phases that we discuss later. Of course, the correct values of u_m, v_m must be obtained by energy minimization i.e. by solving the eigenvalue equation for the Hartree-Fock Hamiltonian of an isolated Skyrmion. This is discussed in Ref. 5. For the same reason, we choose in Eq. (59) a pairing with $\Delta m = -2$ because the vorticity of the Skyrmions we get in our crystals is 4π.

It is clear from Eq. (59) that there are many variations of the microscopic wavefunction $|\mathcal{S}_p\rangle$ that we can make that would lead to pseudospin textures with different topological and real electric charges. A study of these different solutions is, however, beyond the scope of this paper.
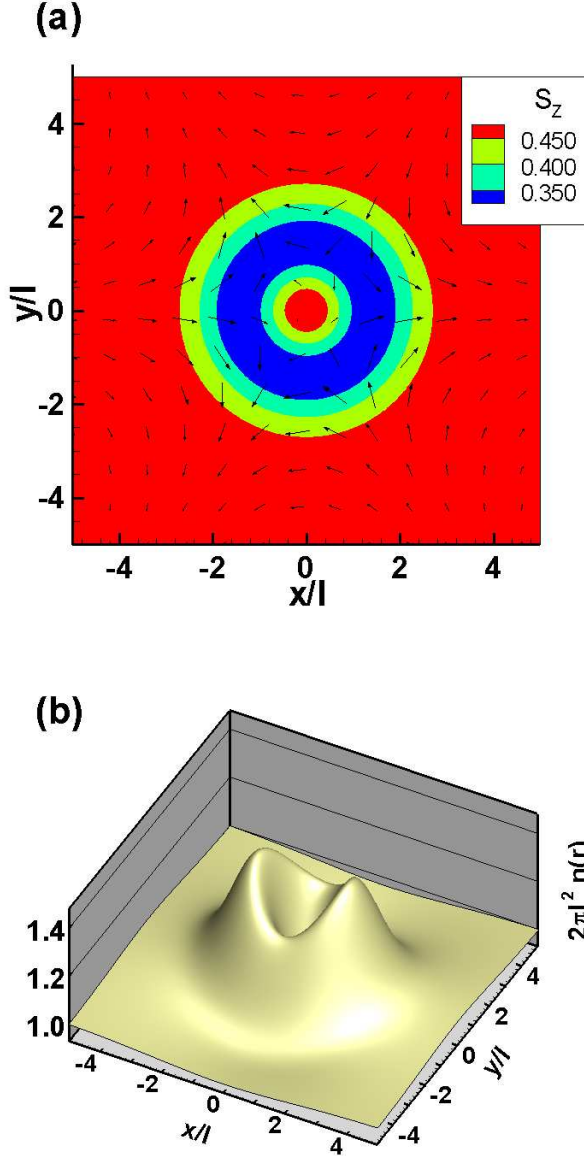
(a)

(b)

FIG. 5: (Color online) An orbital Skyrmion with $p = -1$ added to a filled Landau level for the parameters of Eq. (56) with $\Delta = 0.05$. (a) Orbital pseudospin profile in the RSR. (b) Total density $n(\mathbf{r})$ in the RSR.

C.   Skyrmion energy

Orbital Skyrmions could occur, for example, at $\nu = -3$ when the bias is strong enough for all the charge to be transferred to the state $|K', 0\rangle$. When $\zeta_1 = 0$, this state occurs[2] for $\Delta_B \geq 0.0012 e^2/\kappa\ell$. In this state, the gap between the $n = 0$ and $n = 1$ state, $\beta\Delta_B$, is very small and one would expect orbital Skyrmions, in analogy with spin Skyrmions, to have lower energy than the corresponding electron quasiparticles. The energetics of an orbital

Skyrmion is however different from its spin analog as we now show.

With all electrons in the state $|K', 0\rangle$, the energy per electron is given by

$$
\begin{aligned}
\frac{E}{N_0} &= -\frac{1}{2}\Delta_B - \frac{1}{2}X_{0,0,0,0}(0) \qquad (65) \\
&= -\frac{1}{2}\Delta_B - \frac{1}{2}\sqrt{\frac{\pi}{2}}.
\end{aligned}
$$

The energy needed to remove one electron in orbital m from the ground state (i.e. the energy to create one hole) is given by

$$
E_{hole} = \frac{1}{2}\Delta_B + X_{0,0,0,0}(0), \qquad (66)
$$

while the energy required to add one electron in $n = 1$ is given by

$$
\begin{aligned}
E_e &= -\frac{1}{2}\Delta_B + \beta\Delta_B - X_{0,1,1,0}(0) \qquad (67) \\
&= -\frac{1}{2}\Delta_B + \beta\Delta_B - \frac{1}{2}\sqrt{\frac{\pi}{2}}
\end{aligned}
$$

and is negative at zero bias. The energy to create an electron (in $n = 1$) and hole (with $n = 0$) pair with infinite separation is thus

$$
\Delta_{eh,(orbital)} = E_e + E_{hole} = \beta\Delta_B + \frac{1}{2}\sqrt{\frac{\pi}{2}}. \qquad (68)
$$

Let's compare this result with the energy needed to create an electron (in $n = 0$) and hole (in $n = 0$) pair with different spins i.e.

$$
\Delta_{eh,(spin)} = g\mu_B B + \sqrt{\frac{\pi}{2}}. \qquad (69)
$$

The first term on the right-hand side of this last equation is the Zeeman energy. The energy needed to flip an orbital pseudospin is smaller than the energy to flip a spin (at zero bias and Zeeman couplings). It follows that the condition required to excite a Skyrmion pair i.e. $\Delta_{skyrmion-antiskyrmion} < \Delta_{eh,(orbital)}$ is more restrictive for an orbital Skyrmion than for a spin Skyrmion. $\Delta_{eh,(orbital)} < \Delta_{eh,(spin)}$ because of the presence of the extra exchange energy, $X_{0,1,1,0}(0)$, between different orbitals which is not present in the spin case.

Another important difference between the orbital and spin Skyrmions is that the exchange energy is smaller in $n = 1$ than in $n = 0$ i.e. $X_{1,1,1,1}(0) = \frac{3}{4}X_{0,0,0,0}(0)$. For this reason, the gain in exchange energy obtained by making an orbital pseudospin texture is not as big as for a spin texture.

A detailed numerical calculation of the energy of the Skyrmion and anti-Skyrmion excitations under finite bias thus has to be made in order to compare their energy with those of the electron and hole excitations. This can

by done by energy minimization, using the method described in Ref. 5. Despite our efforts, we have not been able so far to achieve sufficient precision with our numerical code to classify energetically these different solutions. We thus concentrate, in this paper, on crystal solutions which are a lot easier to compute.

We remark that orbital Skyrmions have been studied previously in a conventional semiconductor 2DEG[16]. They were called, in this context, inter-Landau-level Skyrmions and involved spin flips between the $n = 0$ spin down state and the $n = 1$ spin up state. Since there is no exchange energy between states with different spin indices, the energetics of these inter-Landau-level Skyrmions is different from that of our orbital Skyrmions in which orbital pseudospin flips occur between states with the same spin. The conclusion of Ref. 16 that inter-Landau-level Skyrmions are never the lowest lying charged excitation cannot be applied to our system.

VI. SKYRMION CRYSTALS

We now consider the ground state of the 2DEG in bilayer graphene at non integer filling factors $\widetilde{\nu} \in [1, 3]$. We look for crystal solutions of Eq. (25) allowing for the possibility of both valley and orbital pseudospin textures. We do not attempt to make an exhaustive study of the phase diagram of the 2DEG since considering all the possible crystal states would be a formidable task. We restrict ourselves to square and triangular lattices with one and two electrons per unit cell and single out the state with the lowest energy. We take $\zeta_1 = 0$ and discuss the effect of a finite ζ_1 in the conclusion of this paper.

All results presented in this paper are for a magnetic field $B = 10$ T. We measure the energy in units of $e^2/\kappa\ell = 0.036$ eV for $\kappa = 5$ appropriate for graphene on a SiO$_2$ substrate. For the validity of the two-band model used in our calculations, we need $\Delta_B << \gamma_1 = 0.39$ eV i.e. $\Delta_B / (e^2/\kappa\ell) << 11$.

We start by presenting the crystal state at large bias for $\widetilde{\nu}$ around 1 because the Skyrmion at each site is close to the simple solution we presented in Fig. 5 in this case. We then study the crystals for $\widetilde{\nu}$ near 1 and 3. These two filling factors give very similar solutions. We end with filling factor near 2 where radically different solutions are obtained.

A. Orbital Skyrmion crystal at large bias

The simplest crystalline structure occurs at large bias with $\widetilde{\nu}$ around 1. In this case, valley K is empty and the charge is entirely in valley K'. This corresponds to the situation we studied in Sec. V(b). The crystal solution is a triangular lattice of orbital Skyrmions with one Skyrmion per lattice site. We show an example of this solution for $\widetilde{\nu} = 1.2, \Delta_B / (e^2/\kappa\ell) = 1.28$ in Fig. 6. We see that for each Skyrmion in the lattice, the pseudospin and

density profiles (in the RSR) are close to the very crude Skyrmion solution we illustrated in Fig. 5. Note that if we use the GCR instead, the pseudospin and density profile for each Skyrmion are exactly those of the usual spin Skyrmion we illustrated in Fig. 4 i.e. the pseudospins rotates by 2π around the center of the Skyrmion and the pseudospins point downward at the center (we show this in Fig. 7).
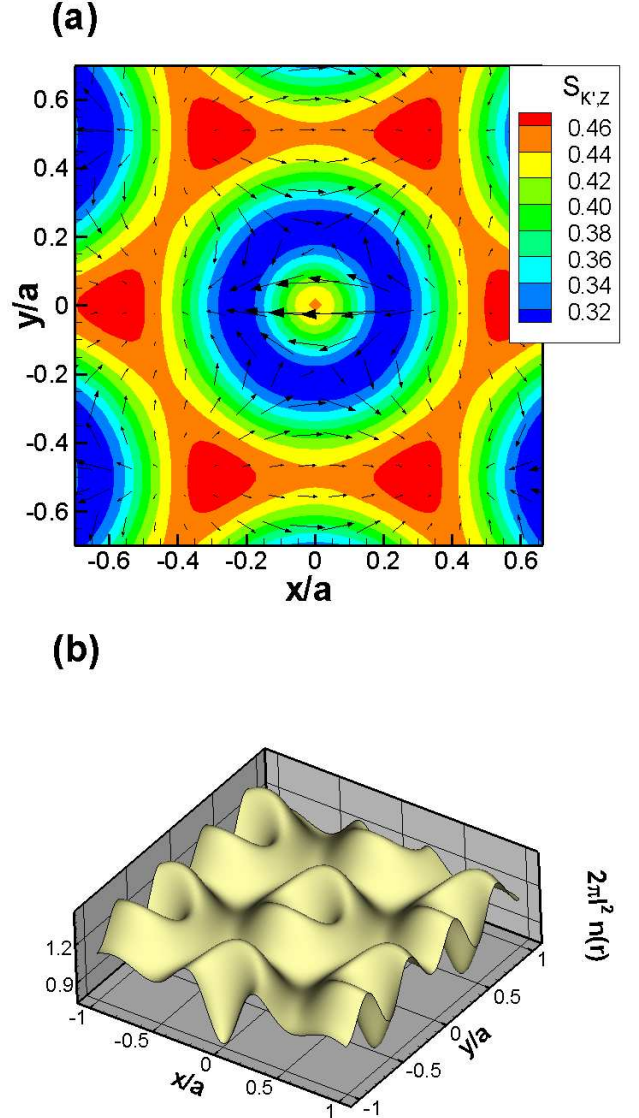

FIG. 6: (Color online) Orbital Skyrmion crystal at $\widetilde{\nu} = 1.2$ and $\Delta_B / (e^2/\kappa\ell) = 1.28$. (a) Pseudospin texture in the RSR. (b) Total density $n(\mathbf{r})$ in the RSR.

The Wigner crystal solution (i.e. no orbital pseudospin texture) can be found if the bias is taken to be extremely large i.e. of the order of $\Delta_B / (e^2/\kappa\ell) \approx 30$ which is

well beyond the limit of validity of our model. If we compare the interaction energy of the Skyrme crystal at $\Delta_B / \left(e^2/\kappa\ell \right) = 1.28$ with that of the Wigner crystal at $\Delta_B / \left(e^2/\kappa\ell \right) = 30$, we find that the energy of the former is lower than that of the later by approximately 0.5%. (The interaction energy includes all terms in Eq. (28) with the exception of the bias energy). The Hartree part of the total energy is bigger in the Skyrme than in the Wigner crystal while the exchange (Fock) energy is more negative in the Skyrme crystal probably because Skyrmions are larger objects and overlap more with their neighbors. It could be also that isolated Skyrmions have lower energy than electron or hole quasiparticles. As mentioned earlier, we have not been able to confirm that Skyrmions have lower energy than isolated electrons and holes in the dilute limit using separate isolated quasiparticle calculations. If indeed Skrymions are only stable beyond a minimum density, the crystal stability must be related to inter-Skyrmion exchange energies

B. Skyrme crystals near $\widetilde{\nu} = 1, 3$ and zero bias

It was shown in Ref. 1 that, in the Hartree-Fock approximation, the ground states of the 2DEG in $N = 0$ at integer filling factors satisfy a set of Hund's rules in which the spin polarization is maximized first, then the layer polarization is maximized to the greatest extent possible, and finally the orbital polarization is maximized to the extent allowed by the first two rules. At zero bias, the ordering of the first four states (with spin up) is given by

$$|S, 0\rangle = \frac{1}{\sqrt{2}} |K, 0\rangle + \frac{1}{\sqrt{2}} |K', 0\rangle, \qquad (70)$$

$$|S, 1\rangle = \frac{1}{\sqrt{2}} |K, 1\rangle + \frac{1}{\sqrt{2}} |K', 1\rangle,$$

$$|AS, 0\rangle = \frac{1}{\sqrt{2}} |K, 0\rangle - \frac{1}{\sqrt{2}} |K', 0\rangle,$$

$$|AS, 1\rangle = \frac{1}{\sqrt{2}} |K, 1\rangle - \frac{1}{\sqrt{2}} |K', 1\rangle,$$

in this order. (The guiding-center index X is left implicit in these equations).

At $\widetilde{\nu} = 1$, the first level is completely filled while at $\widetilde{\nu} = 3$, the first three levels are completely filled. At $\widetilde{\nu} = 1 + x$ with $|x| \lesssim 0.5$, a finite density of electrons ($x > 0$) or holes ($x < 0$), in the $|S, 1\rangle$ or $|S, 0\rangle$ state condense into a crystal phase. At $x = 0.2$ and zero bias, we find that the electrons in the $|S, 1\rangle$ state condense into a triangular crystal with two orbital Skyrmions per site (i.e. one orbital Skyrmions in each layer). There is no layer-pseudospin texture (no pseudospin rotation) in this case since all electrons are in a symmetric state of the bilayer but there is an interlayer coherence. Moreover, an orbital-pseudospin texture is always present.

The crystal state at $\widetilde{\nu} = 3.2$ and zero bias is identical to that at $\widetilde{\nu} = 1.2$ with the exception that it is the electrons in the $|AS, 1\rangle$ that now condense into a crystal phase and orbital Skyrmions are formed by flipping orbital pseudospins from $|AS, 0\rangle$ to $|AS, 1\rangle$. There are again 2 orbital Skyrmions per site. The two states $|S, 0\rangle, |S, 1\rangle$ are completely filled and inert and give a background density of $2/2\pi\ell^2$. The pseudospin and density patterns in the RSR and GSR for this crystal state with lattice spacing a are shown in Fig. 7. (In these figures, a is the Skyrmion lattice constant and $a >> a_0$). The pseudospin pattern for $S_{K,Z}$ (not shown in the figure) is identical to that of $S_{K',Z}$. The additional central peak in the RSR density profile occurs because there are 2 Skyrmions per site in this crystal. Note that the pseudospin for the charge $q = 2e$ Skyrmion rotates by 4π in the RSR but only 2π in the GCR.

C. Bias $\Delta_B > \Delta_B^{(c)}$

With finite bias, the charge in layer K is progressively transferred to layer K'. For the crystal states discussed above, that means that the size of the Skyrmions decreases in layer K and increases in layer K'. In our mean-field approximation, the charge of the Skyrmions is not quantized and the crystal states can be seen as exotic charge density waves with complex pseudospin textures. Above a very small bias of order $\Delta_B^{(c)} / \left(e^2/\kappa\ell \right) \approx 0.0011$ at $\widetilde{\nu} = 1$, all electrons are pushed into the $|K', 0\rangle$ valley and interlayer coherence is lost. The ordering of the energy levels at $\widetilde{\nu} = 1$ is then given by $|K', 0\rangle, |K', 1\rangle, |K, 0\rangle, |K, 1\rangle$ and the ground state has all electrons in $|K', 0\rangle$. At $\widetilde{\nu} = 1.2$ and $\Delta_B / \left(e^2/\kappa\ell \right) = 0.002$, we find a triangular crystal of orbital Skyrmions in layer K' with again two electrons per site. There are no electrons in valley K. The guiding-center density and vector fields patterns for this state are given in Fig. 8. The total density is identical to that of the crystal state found at zero bias (see Fig. 7) but it is now completely in layer K' instead of being equally shared between the two layers. The orbital pseudospin pattern in K' is the sum of the orbital pseudospin patterns found in each layer at zero bias.

The pseudospin texture and density for a single orbital Skyrmions of charge $q = 2e$ on each site of the lattice in Fig. 7 can be obtained with the microscopic expression

$$\left| \mathcal{S}^{(2e)} \right\rangle = \prod_{m=0}^{\infty} \left[-u_m c_{1,m+2}^\dagger + v_m c_{0,m}^\dagger \right] c_{1,0}^\dagger c_{1,-1}^\dagger |0\rangle. \qquad (71)$$

The density in this state is given by

$$n_1^{(2e)} (\mathbf{r}) = |\phi_{1,-1} (\mathbf{r})|^2 + |\phi_{1,0} (\mathbf{r})|^2 \qquad (72)$$
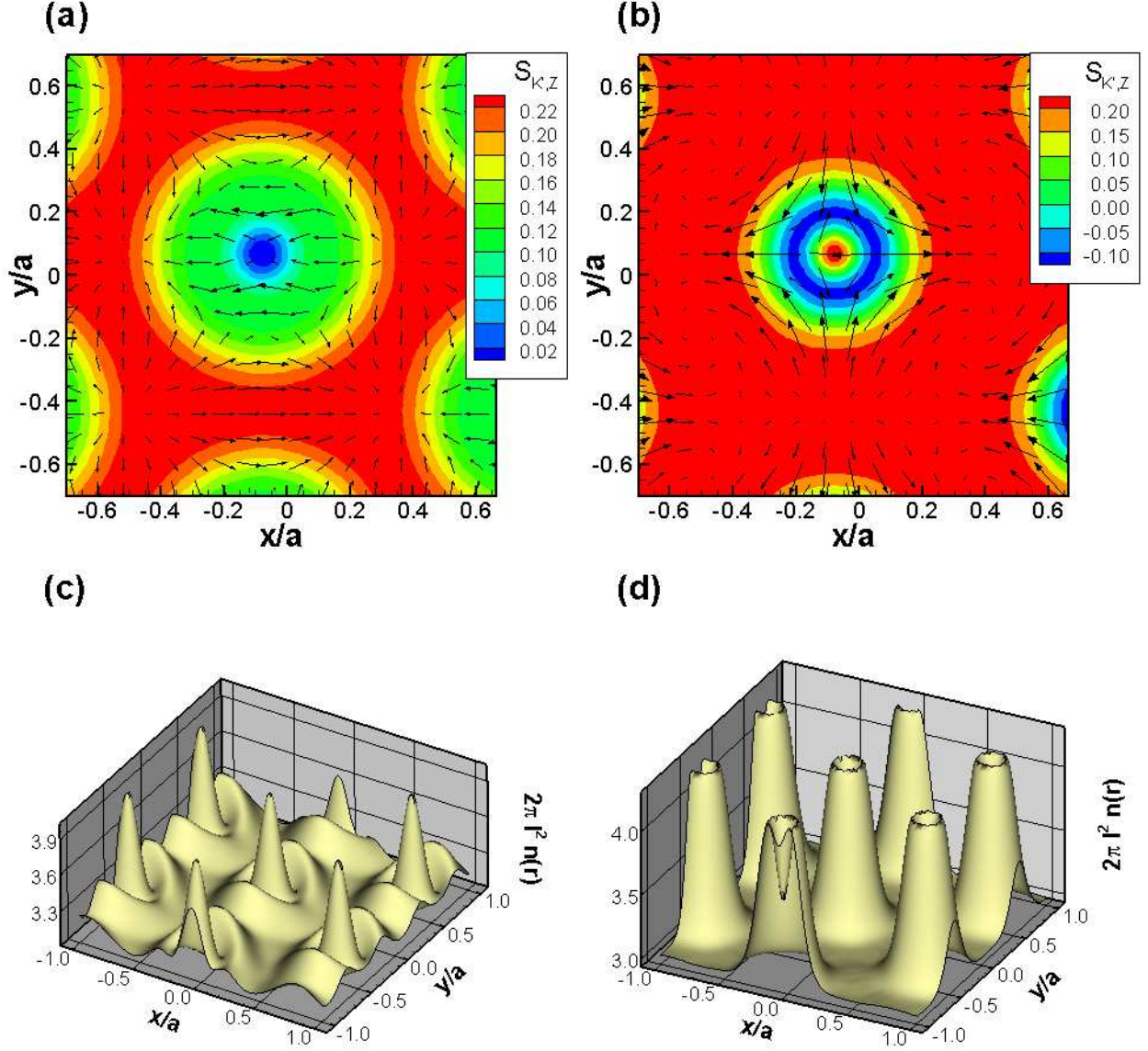$$+ \sum_{m=0}^{\infty} |h_{1,m+2} (\mathbf{r})|^2 |v_m|^2,$$

FIG. 7: (Color online) Orbital Skyrmion crystal at $\widetilde{\nu} = 3.2$ and $\Delta_B / \left(e^2/\kappa\ell \right) = 0$. (a) Orbital pseudospin texture in the RSR. (b) Orbital pseudospin texture in the GCR. (c) Total density $n\left(\mathbf{r}\right)$ in the RSR. The pseudospin pattern for $S_{K,Z}$ (not shown) is identical to that of $S_{K',Z}$. (d) Total density $\widetilde{n}\left(\mathbf{r}\right)$ in the GCR. The lattice constant is a.

while the pseudospin texture is still given by Eq. (60) and

$$S_z^{(2e)}\left(\mathbf{r}\right) = \frac{1}{2}\left[n_0\left(\mathbf{r}\right) - n_1^{(2e)}\left(\mathbf{r}\right) \right]. \tag{73}$$

The phase diagram of the liquid state at $\widetilde{\nu} = 3$ is richer than at $\widetilde{\nu} = 1$ since a mixed state with both orbital and interlayer coherences is possible[3] due to the fact that the kinetic energy contribution $-\beta_0 \Delta_B$ in Eq. (8) is negative and so decreases the exchange-enhanced gap $\Delta^* = E_{n=0} < E_{n=1}$ with increasing bias. (This gap Δ^* is positive at zero bias but changes sign at sufficiently high bias). In the region with orbital coherence only,

i.e. for $\Delta_B / \left(e^2/\kappa\ell \right) \gtrsim 0.0022$, the ordering of the levels is given by $|K',0\rangle, |K',1\rangle, |K,B\rangle, |K,AB\rangle$ where B and AB represent bonding and anti-bonding combinations of the $n = 0$ and $n = 1$ states defined by

$$|K,B\rangle = \sqrt{1-\sigma}\,|K,0\rangle + \sqrt{\sigma}\,|K,1\rangle, \tag{74}$$
$$|K,AB\rangle = -\sqrt{\sigma}\,|K,0\rangle + \sqrt{1-\sigma}\,|K,1\rangle, \tag{75}$$

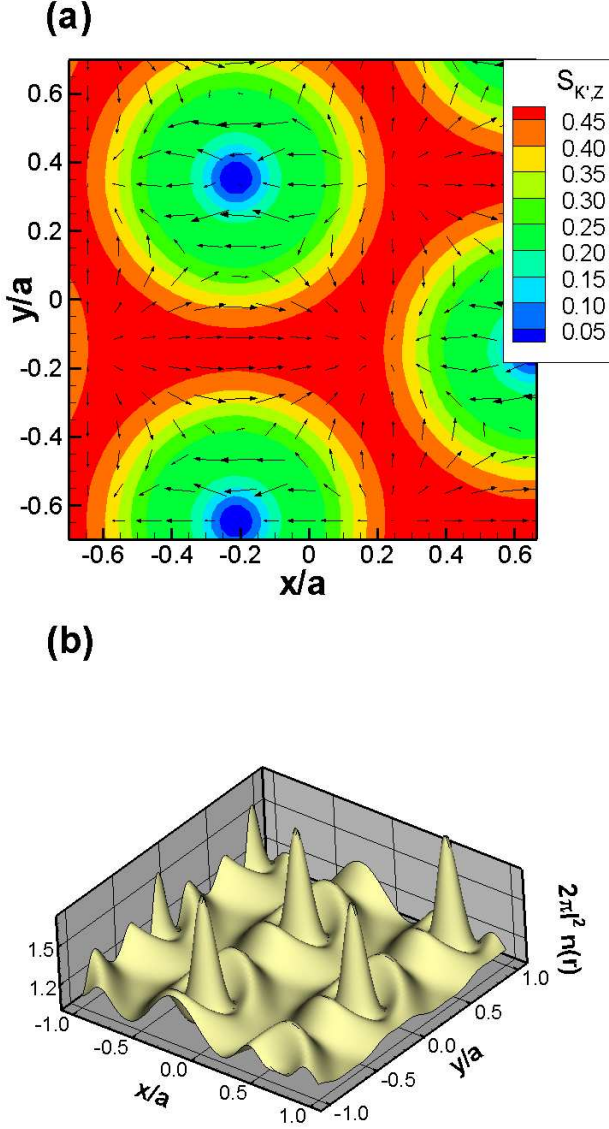with

$$\sigma = \frac{\Delta_B}{\Delta_B^{(2)}}, \tag{76}$$

(a)

(b)

FIG. 8: (Color online) Orbital Skyrmion crystal at $\widetilde{\nu} = 1.2$ and $\Delta_B/\left(e^2/\kappa\ell\right) = 0.002$. (a) Orbital pseudospin texture in the RSR. (b) Total density $n\left(\mathbf{r}\right)$ in the RSR. The pseudospin $\mathbf{S}_K = 0$.

and

$$\Delta_B^{(2)} = \frac{1}{4\beta}\sqrt{\frac{\pi}{2}} \approx 5\frac{e^2}{\kappa\ell} \tag{77}$$

(at $B = 10$ T) is the bias at which the electrons are completely transferred to the state $|K,1\rangle$ at $\widetilde{\nu} = 3$. The two levels $|K',0\rangle, |K',1\rangle$ are completely filled. The number of electrons in state $|K,1\rangle$ is given by

$$\nu_{K,1} = \frac{\Delta_B}{\Delta_B^{(2)}}. \tag{78}$$

At $\widetilde{\nu} = 3.2$ and $\Delta_B \gtrsim \Delta_B^{(c)}$ (with $\Delta_B^{(c)} = 0.0021$, we get a triangular crystal of orbital Skyrmions with charge $q = -2e$ per site with a density and pseudospin patterns in the $n = 0, 1$ basis similar to those represented in Fig. 8. The only difference with the $\widetilde{\nu} = 1.2$ case is that Skyrmions are now made from a filled $|K, B\rangle$ level by flipping pseudospins to the $|K, AB\rangle$ level. When Δ_B is close to $\Delta_B^{(c)}$, however, electrons are in majority in level $n = 0$ and there is not much difference with the $\widetilde{\nu} = 1.2$ case. When the bias is sufficiently strong for the exchange-enhanced gap to be negative, the crystal phase is much more complex but the orbital pseudospin texture persists. We do not discuss this limit further in this paper.

Skyrmion with charge $q = -2e$ are not unknown. It was shown in Ref. 17, for example, that at small density, there is an attractive force between two Skyrmions with opposite global phases of their spin component that goes like $1/R$ where R is the separation between the two Skyrmions. At large separation R, this force prevails over Coulomb repulsion. Also, in previous studies of spin and pseudospin Skyrmions in conventional semiconductor's 2DEG, it was found that lattice with pairs of Skyrmions occurred for small value of the Zeeman or bias couplings[12].

D. Skyrme crystals near $\widetilde{\nu} = 2$

At $\widetilde{\nu} = 2$, the uniform ground state at zero bias has interlayer coherence in $n = 0$ *and* in $n = 1$ so that the first two states in Eqs. (70) are filled. Above a critical bias of the order of $\Delta_B^{(c)}/\left(e^2/\kappa\ell\right) \approx 0.003$, all charge are transferred to the K' valley and states $n = 0$ and $n = 1$ are then fully occupied. Interlayer as well as orbital coherences are lost.

At $\widetilde{\nu} = 2.2$ and zero bias, the electronic phase consists of two layer-pseudospin meron crystals with each meron carrying charge $q = -e/2$. There is a meron texture in $\mathbf{P}_0$ and in $\mathbf{P}_1$. This phase is depicted in Fig. 9. The merons are arranged in a checkerboard configuration with 8 merons per unit cell (the total charge in one unit cell is $4e$). The layer-pseudospins in the central meron are rotated by a phase π with respect to the merons at the corner of the unit cell. The orbital coherence is more than ten time smaller than the interlayer coherence and can be neglected.

The charge in the pseudospin merons with pseudospin down (up) at the center progressively decreases (increases) when the bias is increased. For $\widetilde{\nu} = 2.2$ and at $\Delta_B/\left(e^2/\kappa\ell\right) \approx 0.007$, we find that there is a phase transition to a state where the two states in valley K'
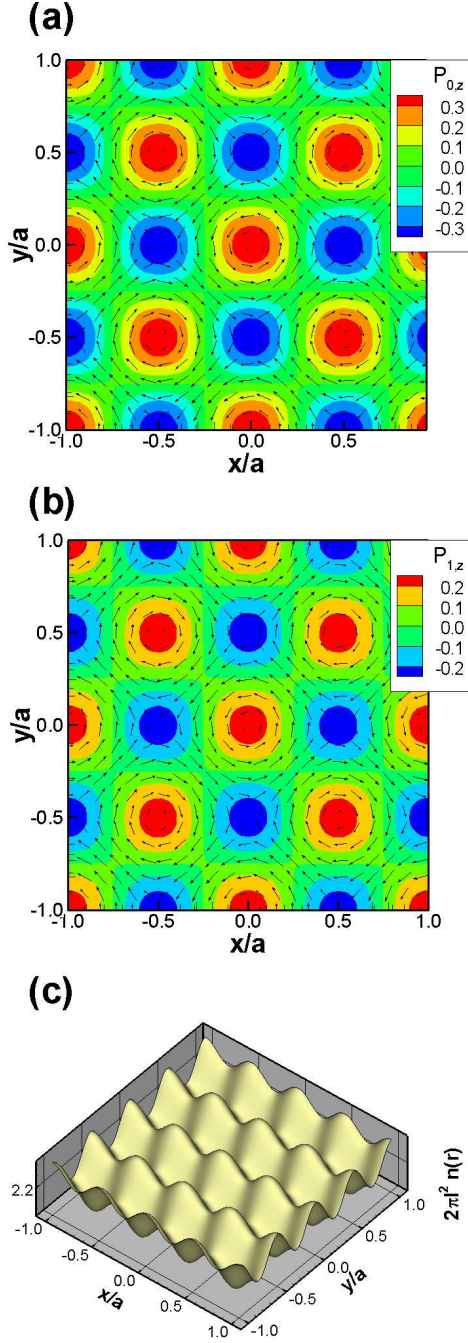
(a)

(b)

(c)

FIG. 9: (Color online) Interlayer Skyrmion crystal at $\widetilde{\nu} = 2.2$ and $\Delta_B / \left(e^2 / \kappa \ell \right) = 0$.(a) Layer-pseudospin texture in $n = 0$ and (b) Layer-pseudospin texture $n = 1$ in the RSR. (c) Total density $n \left(\mathbf{r} \right)$ in the RSR.

are completely filled and the remaining electrons crystallize in the K valley. In the $n = 0, 1$ basis, this gives a triangular crystal with one electron per site and an orbital pseudospin vortex around each electron. Note that the liquid phase at $\widetilde{\nu} = 2$ has all electrons in a bonding

state $|K, B\rangle$ of Eq. (74) (with $\Delta_B^{(2)} = (\widetilde{\nu} - 1)\sqrt{\pi/2}/4\beta$ in this case) and we could have expected a Wigner crystal phase with electrons in the $|K, B\rangle$ state at each site. It seems however that the system again prefers to form a pseudospin texture at each site. This crystal state is represented in Fig. 10.
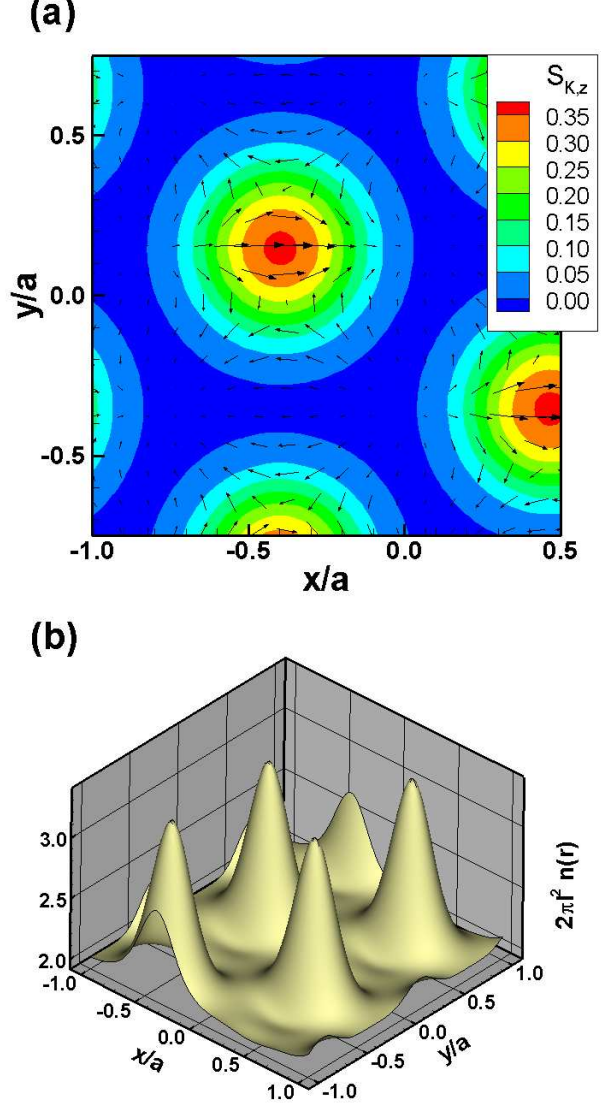

(a)

(b)

FIG. 10: (Color online) Orbital crystal at $\widetilde{\nu} = 2.2$ and $\Delta_B / \left(e^2 / \kappa \ell \right) = 0.007$. (a) Orbital pseudospin texture in the RSR. (b) Total density $n \left(\mathbf{r} \right)$ in the RSR.

As in the $\widetilde{\nu} = 3.2$ case discussed above, the exchange-enhanced gap Δ^* between $n = 0$ and $n = 1$ is of the order of $e^2 / \kappa \ell$ at $\widetilde{\nu} = 2$. The contribution $-\beta_0 \Delta_B$ (see Eq. (8)) decreases this gap as Δ_B is increased. This increases the number of flipped orbital pseudospins. At

$\Delta_B^{(2)} = (\widetilde{\nu} - 1)\sqrt{\pi/2}/4\beta$, there is a transition to a Wigner crystal with all electrons in $n = 1$ at each site and there is no pseudospin texture anymore.

It is possible to find another interesting solution with our numerical code at $\Delta_B > \Delta_B^{(c)}$ that has, however, an higher energy than that of Fig. 10. We mention it here because it is closely related to the work reported in Ref. 6. This solution is a crystal of layer-pseudospin Skyrmions in $n = 0$ and in $n = 1$ with a charge $q = -2e$ Skyrmion at each crystal site. This solution is the natural extension of the solution at zero bias since the bias transfers the charge of half the merons in one layer to the other half in the same layer. This structure is shown in Fig. 11. We remark that our convention for the *interlayer* pseudospin is that state up corresponds to valley K. Since the charge is pushed in valley K' with positive bias, the majority state is pseudospin down. In that case, a Skyrmion has spin up at the center and spin down away from the center.

This type of solution i.e. Skyrmions with a superposition of $n = 0$ and $n = 1$ interlayer textures have been studied by Abanin et al.[6] (the small contribution $\beta_0 \Delta_B$ to the gap was set to zero in that paper). These authors concluded that such charge $q = -2e$ Skyrmions would have lower energy than electron or hole quasiparticles at filling factor $\widetilde{\nu} = 2.0$. The crystal structure that we get is consistent with their finding but it is not the ground state. As we mentioned before, our conclusions for the crystal state do not necessarily apply to the case of an isolated Skyrmion. If we define a Skyrmion creation operator in states $n = 0, 1$ as

$$d_0^\dagger = \prod_{m=0}^{\infty} \left[-u_{0,m} c_{K,0,m+1}^\dagger + v_{0,m} c_{K',0,m}^\dagger \right] c_{K,0}^\dagger \, |0\rangle , \quad (79)$$

$$d_1^\dagger = \prod_{m=-1}^{\infty} \left[-u_{1,m} c_{K,1,m+1}^\dagger + v_{1,m} c_{K',1,m}^\dagger \right] c_{K,-1}^\dagger \, |0\rangle , \quad (80)$$

then the $2e$ Skyrmion state can be written as

$$\left| \mathcal{S}^{(2e)} \right\rangle = d_1^\dagger d_0^\dagger \, |0\rangle \quad (81)$$

and the angular momentum pairing is such that $m_{K'} - m_K = 1$ for both Skyrmions.

In a previous publication[3], we derived an effective model for the orbital pseudospin-wave excitations at $\widetilde{\nu} = 3$. This effective model had in it a Dzyaloshinskii-Moriya interaction. This type of interaction favors the formation of spiral or vortex states. We see that this term is also at work in the crystal states.

VII. TOTAL AND LOCAL DENSITY OF STATES

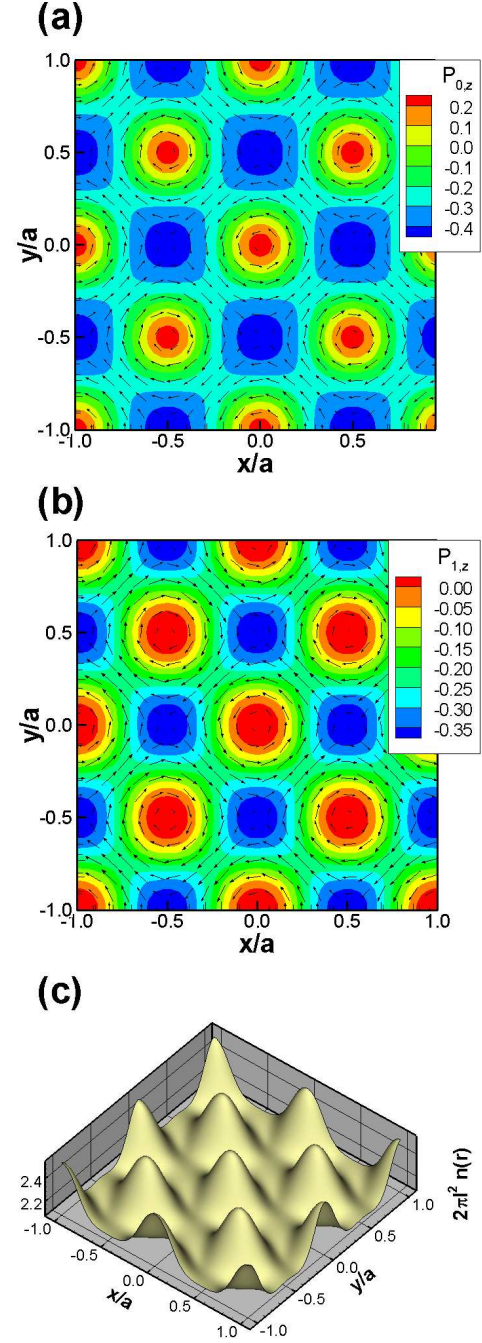Skyrmion lattices with charge $q = -2e$ can be distinguished from Skyrmion lattices with charge $q = -e$ by

FIG. 11: (Color online) Interlayer-Skyrmion crystal at $\widetilde{\nu} = 2.2$ and $\Delta_B / \left(e^2/\kappa\ell \right) = 0.03$. (a) Layer-pseudospin texture in $n = 0$ and (b) $n = 1$ in the RSR. (c) Total density $n(\mathbf{r})$ in the RSR. Note that the majority state is pseudospin down. This state is not the ground state in our numerical calculation.

their total density of states (TDOS) which is defined by

$$g_T(\omega) = -\frac{1}{\pi} \sum_{n,a} \int d\mathbf{r} \, \mathrm{Im} \left[G_{n,n}^{(R)a,a}(\mathbf{r},\mathbf{r},\omega) \right] \quad (82)$$

$$= -\frac{N_\phi}{\pi} \sum_{n,a} \mathrm{Im} \left[G_{n,n}^{(R)a,a}(\mathbf{q}=0,\omega) \right],$$

where $G_{n,n}^{(R)a,a}$ (with $a = K, K'$ and $n = 0,1$) is the retarded single-particle Green's function which is related to the Matsubara Green's function defined in Eq. (23) by $G_{n,n}^{a,a}(\mathbf{q}, i\omega_n \to \omega + i\delta) = G_{n,n}^{(R)a,a}(\mathbf{q},\omega)$.
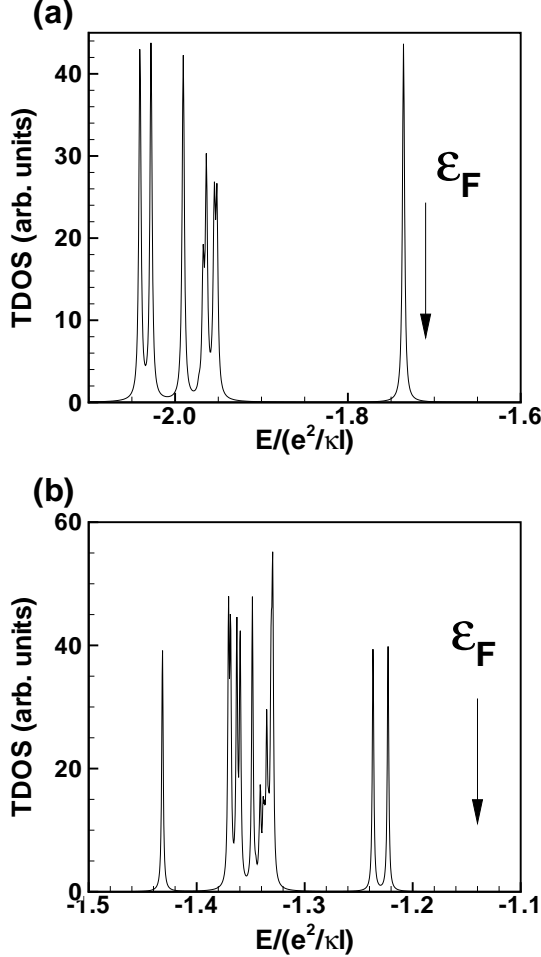
(a)

(b)

FIG. 12: Total density of states for orbital Skyrmion crystals at $\widetilde{\nu} = 1.2$. (a) For $\Delta_B/\left(e^2/\kappa\ell\right) = 1.28$. Skyrmions with $q = -e$. (b) For $\Delta_B/\left(e^2/\kappa\ell\right) = 0.002$. Skyrmions with $q = -2e$. Only the low-energy part of the TDOS is shown in these figures.

The number of peaks near the Fermi level in the TDOS is equal to the number of electrons in a Skyrmion. This is illustrated in Fig. 12 where we show the low-energy part of $g_T(\omega)$ corresponding to the crystals of Fig. 6 ($q = -e$ Skyrmion at each site) and Fig. 7 ($q = -2e$ Skyrmion at each site). A similar result was also found for bubble crystals in semiconductor's 2DEG[18].

It was shown by Poplavskyy et al.[19] that the density pattern in the bubble crystal can also be seen by scanning tunneling microscopy. This measure is related to the *local* density of states (LDOS) which is defined by

$$g_L(\mathbf{r},\omega) = -\frac{1}{\pi} \sum_{n,a} \mathrm{Im} \left[G_{n,n}^{(R)a,a}(\mathbf{r},\mathbf{r},\omega) \right], \quad (83)$$

$$= -\frac{1}{\pi S} \sum_{n,a} \sum_{\mathbf{q}} \mathrm{Im} \left[\widehat{G}_{n,n}^{(R)a,a}(\mathbf{q},\omega) e^{-i\mathbf{q}\cdot\mathbf{r}} \right],$$

where

$$\widehat{G}_{n,n}^{a,a}(\mathbf{q},\omega) \equiv \int d\mathbf{r} e^{i\mathbf{q}\cdot\mathbf{r}} G_{n,n}^{(R)a,a}(\mathbf{r},\mathbf{r},\omega), \quad (84)$$

$$= N_\phi G_{n,n}^{a,a}(-\mathbf{q},\omega) K_{n,n}(\mathbf{q}).$$

We show in Fig. 13 the LDOS in valley K' evaluated at the energy of the two highest-energy peaks in Fig. 12(a) and at the highest-energy peak in Fig. 12(b). The LDOS is almost the same for both peaks in the case of the Skyrmion crystal with charge $q = -2e$. The LDOS for the Skyrmion crystal with charge $q = -e$ looks much the same. Following Ref. 19, we can also sum the LDOS evaluated at all the peaks below the Fermi energy. It is easy to show analytically, using Eq. (24), that this summation gives

$$\int_{-\infty}^{E_F} g_L(\mathbf{r},\omega) \, d\omega = N_p(\mathbf{r}), \quad (85)$$

where $N_p(\mathbf{r})$ is the density we defined in Sec. V(b). This density is actually quite close to the real space density $n(\mathbf{r})$ that we plotted in many of the figures of this paper (it does not contain the term $2\mathrm{Re}\left[S_-(\mathbf{r})\right]$).

VIII. ELECTRIC DIPOLE TEXTURES

Apart from the minus sign in front of $\langle \rho_{a,y}(\mathbf{G}) \rangle$ in Eq. (41), the vector field representation for the electric dipoles in the crystal states with orbital coherence is just like the GCR of the orbital pseudospin field $\mathbf{S}_{a,\perp}(\mathbf{r})$ where $a = K, K'$. We give an example of the dipole field in Fig. 7 for the charge $q = -2e$ orbital Skyrmion crystal at $\widehat{\nu} = 3.2$ and bias $\Delta_B/\left(e^2/\kappa\ell\right) = 0$. The rotation of the pseudospins is 2π for both charge $q = -e$ and charge $q = -2e$ Skyrmions so that the $\mathbf{S}_{a,\perp}$ field pattern does not allow to discriminate between these two types of crystals.

From Eq. (40), we see that in the presence of an external uniform electric field $\mathbf{E} = E_{0x}\widehat{\mathbf{x}} + E_{0y}\widehat{\mathbf{y}}$ in the plane of the layers, the coupling with the electron gas is given by

$$H_{ext} = \sqrt{2}\ell e N_\varphi \int d\mathbf{r} \left(E_{0,x}\overline{\rho}_{j,x}(\mathbf{r}) - E_{0,y}\overline{\rho}_{j,y}(\mathbf{r}) \right) \quad (86)$$

$$= -\sqrt{2}\ell e N_\varphi \left(E_{0,x}\rho_{j,x}(\mathbf{G}=\mathbf{0}) - E_{0,y}\rho_{j,y}(\mathbf{G}=\mathbf{0}) \right).$$

(a) $E/(e^2/\kappa l) = -1.22$

(b) $E/(e^2/\kappa l) = -1.24$

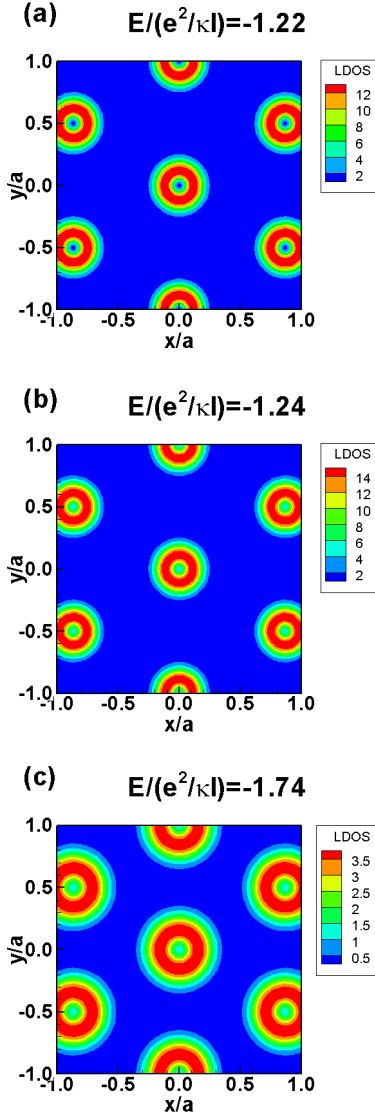**(c)** $E/(e^2/\kappa l) = -1.74$

FIG. 13: (Color online) Local density of state (LDOS) in valley K' for the orbital Skyrmion crystals considered in Fig. 12 (a) and (b). (a) and (b) LDOS for the two higher-energy peaks of the crystal with 2 electrons per site. (c) LDOS at the higher-energy peak for the crystal with one electron per site.

In the liquid phase where the orientation of the orbital pseudospins in the $x - y$ plane is arbitrary, this term allows us to rotate the orbital pseudospins in that plane. For a Skyrmion crystal, the effect may be more complex. The parallel electric field forces the orbital pseudospin in the $x - y$ plane and so should increase orbital coherence. It should also change the form of the orbital pseudospin texture of the Skyrmions, orienting them more towards the x axis.

IX. CONCLUSION

We have presented in this paper a study of some crystal phases with valley and/or orbital pseudospin textures that can occur in bilayer graphene away from integer filling factors in Landau level $N = 0$. Our calculations are, strictly speaking, valid within the two-band tight-binding model introduced in Sec. II and within the Hartree-Fock approximation.

In our numerical calculatons, we have neglected the terms β_4 and Δ in Eq. (1). These terms change the gap between the two orbital states $n = 0$ and $n = 1$ to $\zeta_1 - \beta_0\Delta_B$ in the K valley and to $\zeta_1 + \beta_0\Delta_B$ in the K' valley (see Fig. 2). As we mentioned in Sec. II, the value of ζ_1 is not known precisely. If we take the values for β_0, β_4 and Δ cited in Sec. II, we find $\zeta_1/\left(e^2/\kappa\ell\right) = 0.113$ at $B = 10$ T so ζ_1 is probably not small. Since the critical bias needed to push the charge in one layer is such that $\beta_0\Delta_B^{(c)}/(e^2/\kappa\ell) \approx 0.177 \times 10^{-3}$, we see that these additional terms have the possibility to change the phase diagram in an important way especially the phases at small or zero bias. Furthermore, the orbital coherence depends on the gap between the two orbital state. With the value of ζ_1 cited above, the bias Δ_B needed to place the orbital $n = 1$ below $n = 0$ in the valley K is $\Delta_B \approx 1.27$ i.e. a large value. Fortunately, our numerical calculations show that the orbital Skyrmions crystal (which is the most important state we discussed in this paper) does survive in the phase diagram even with a finite ζ_1. At filling factor $\widetilde{\nu} = 1.2$, the additional gap suppress the $q = -2e$ orbital Skyrmion crystal in favor of a $q = -e$ orbital Skyrmion crystal. This is consistent with our mention in Sec. VI (b) that Skyrmion with $q = -2e$ are found at small gap. At filling factor $\widetilde{\nu} = 3.2$, the gap $\zeta_1 - \beta_0\Delta_B$ can be made small (or even negative) and orbital Skyrmion crystals of both types are found.

Skyrmion crystals have both phonon and spin (or pseudospin) wave modes. In Ref. 20, it was shown that the classical (or quantum mean-field) energy of the Skyrmion is independent of the angle φ which defines the global XY orientation of the spin components. This extra $U(1)$ degree of freedom for a single Skyrmion leads to a broken symmetry in the crystal ground state and hence to a spin wave mode which remains gapless in the presence of a Zeeman field. We expect a similar gapless mode for a crystal of orbital Skyrmions. Fluctuations due to phonons and to these gapless pseudospin modes will have to be considered at finite temperature in order to evaluate the stability of the crystal structures discussed in the present paper.

1 Yafis Barlas, R. Côté, K. Nomura, and A. H. MacDonald, Phys. Rev. Lett. **101**, 097601 (2008).

2 Yafis Barlas, R. Côté, J. Lambert, and A. H. MacDonald, Phys. Rev. Lett. **104**, 096802 (2010).

3 R. Côté, Jules Lambert, Yafis Barlas, and A. H. MacDonald, Phys. Rev. B **82**, 035445 (2010).

4 For a review of spin and pseudospin Skyrmions in semiconductor's 2DEG, see Z. F. Ezawa, *Quantum Hall effects* (World Scientific, Singapore, 2000).

5 H. A. Fertig, L. Brey, R. Côté, and A. H. MacDonald, Phys. Rev. B **50**, 11018 (1994).

6 D. A. Abanin, S. A. Parameswaran, and S. L. Sondhi, Phys. Rev. Lett. **103**, 076802 (2009); D. Lilliehöök, K. Lejnell, A. Karlhede, and S. L. Sondhi, Phys. Rev. B **56**, 6805 (1997).

7 A. H. Castro Neto, F. Guinea, N. M. R. Peres, K. S. Novoselov, A. K. Geim, Rev. Mod. Phys. **81**, 109 (2009).

8 E. McCann and V. I. Fal'ko, Phys. Rev. Lett. **96**, 086805 (2006); E. McCann, Phys. Rev. B **74**, 161403(R) (2006).

9 Eduardo V. Castro, K. S. Novoselov, S. V. Morozov, N. M. R. Peres, J. M. B. Lopes dos Santos, Johan Nilsson, F. Guinea, A. K. Geim, and A. H. Castro Neto, J. Phys.: Condens. Matter **22** (2010) 175503 (2010).

10 René Côté and A. H. MacDonald, Phys. Rev. Lett. **65**, 2662 (1990); R. Côté and A. H. MacDonald, Phys. Rev. B **44**, 8759 (1991).

11 S. Ghosh and R. Rajaraman, Phys. Rev. B **63**, 035304 (2000).

12 J. Bourassa, B. Roostaei, R. Côté, H. A. Fertig, and K. Mullen, Phys. Rev. B **74**, 195320 (2006).

13 C.-H. Zhang and Yogesh N. Joglekar, Phys. Rev. B **75**, 245414 (2007); C.-H. Zhang and Yogesh N. Joglekar, Phys. Rev. B **77**, 205426 (2008).

14 R. Côté, J.-F. Jobidon, and H. A. Fertig, Phys. Rev. B **78**, 085309 (2008).

15 K. Shizuya, Phys. Rev. B **79**, 165402 (2009).

16 D. Lilliehöök, Phys. Rev. B **62**, 7303 (2000).

17 Yu. V. Nazarov and A. V. Khaetskii, Phys. Rev. Lett. **80**, 576 (1998).

18 R. Côté, C. B. Doiron, J. Bourassa, and H. A. Fertig, Phys. Rev. B **68**, 155327 (2003).

19 O. Poplavskyy, M. O. Goerbig, and C. Morais Smith, Phys. Rev. B **80**, 195414 (2009).

20 R. Côté, A. H. MacDonald, Luis Brey, H. A. Fertig, S. M. Girvin, and H. T. C. Stoof, Phys. Rev. Lett. **78**, 4825 (1997).